Physics-Based 3D End-to-End Modeling for Double-RIS Assisted Non-Stationary UAV-to-Ground Communication Channels

Hao Jiang, *Member, IEEE*, Baiping Xiong, Hongming Zhang, *Member, IEEE*, and Ertugrul Basar, *Fellow, IEEE*

***Abstract*— In this paper, we propose a three-dimensional (3D) physics-based double reconfigurable intelligent surface (RIS) cooperatively assisted multiple-input multiple-output (MIMO) stochastic channel model for unmanned aerial vehicle (UAV)-to-ground communication scenarios. The double-RIS is distributed on the surface of buildings can assist the UAV transmitter to reflect its own signals to the ground receiver (GR), and simultaneously enhance the propagation by passive beamforming on the RISs. In the proposed channel model, we derive the *path power gains* for different propagation links between the UAV and GR, thus enabling the proposed channel model to effectively characterize both large- and small-scale fading characteristics of realistic UAV-to-ground communication systems. Furthermore, we derive the critical propagation properties of the proposed channel model, including the spatial cross-correlation functions (CCFs), temporal auto-correlation functions (ACFs), and frequency correlation functions (FCFs), with respect to different RIS reflection phase configurations as well as different RIS orientation angles. Numerical simulation results demonstrate the propagation characteristics of the proposed double-RIS assisted UAV-to-ground channel model behave better than those of traditional channel models with single-RIS link or LoS link, thereby validating the necessity of introducing double-RIS into UAV-to-ground communication.**

***Index Terms*— Reconfigurable intelligent surface, UAV communications, path power gains, end-to-end channel model, propagation characteristics.**

Manuscript received 17 November 2022; revised 5 March 2023; accepted 4 April 2023. Date of publication 13 April 2023; date of current version 17 July 2023. This work is supported by NSFC projects (62001056 and 62101275), Jiangsu NSF project (BK20200820), and Scientific and Technological Research Council of Turkey (TUBITAK) under Grant 120E401. The associate editor coordinating the review of this article and approving it for publication was D. W. K. Ng. *(Corresponding author: Hongming Zhang.)*

Hao Jiang is with the School of Artificial Intelligence/School of Future Technology, Nanjing University of Information Science and Technology, Nanjing 210044, China, and also with the National Mobile Communications Research Laboratory, Southeast University, Nanjing 210096, China (e-mail: jianghao@nuist.edu.cn).

Baiping Xiong is with the National Mobile Communications Research Laboratory, Frontiers Science Center for Mobile Information Communication and Security, Southeast University, Nanjing 210096, China, and also with the Pervasive Communication Research Center, Purple Mountain Laboratories, Nanjing 211111, China (e-mail: xiongbp@seu.edu.cn).

Hongming Zhang is with the College of Information and Communication Engineering, Beijing University of Posts and Telecommunications, Beijing 100876, China (e-mail: zhanghm@bupt.edu.cn).

Ertugrul Basar is with the Communications Research and Innovation Laboratory (CoreLab), Department of Electrical and Electronics Engineering, Koç University, Sariyer, 34450 Istanbul, Turkey (e-mail: ebasar@ku.edu.tr).

Color versions of one or more figures in this article are available at https://doi.org/10.1109/TCOMM.2023.3266832.

Digital Object Identifier 10.1109/TCOMM.2023.3266832

I. Introduction

TO SATISFY the growing demand for applications with global coverage, the sixth generation (6G) wireless communication networks will not be restricted to terrestrial wireless communication, but need to be complemented with non-terrestrial facilities like unmanned aerial vehicles (UAVs) and satellites to create a space-air-ground integrated network (SAGIN) [1]. As an integral part of SAGIN, communication assisted by drones has been evolving rapidly due to their attractive features, such as on-demand deployment, fully controllable mobility, and low cost. However, when the UAV and ground receiver (GR) are deployed in crowded communication areas, the propagation links will be easily blocked by obstructions, like tall trees and buildings, which greatly influence the effective coverage area and channel communication quality. To overcome this shortcoming, reconfigurable intelligent surface (RIS), which consists of an electromagnetic material surface composed of a large number of square metal patches, can be positioned on building walls to manipulate impinging waves towards destinations constructively in an energy-efficient and cost-effective way [2]. Thus, the RIS-assisted UAV communication has attracted extensive attention from both academic and industrial circles.

In practice, channel models are of the vital importance to the design, optimization, and performance evaluation of UAV-to-ground communication systems. Hence, it is critical to propose an end-to-end channel model that can reflect faithfully the impact of the physical properties of RIS on the electromagnetic waves in a wireless environment between the UAV transmitter and GR [3]. In existing literature, channel models are mainly separated into deterministic and stochastic ones. The former ones, such as the ray-tracing method, are generally necessitates conducting a variety of measurements to identify the field strength and propagation path of radio waves. Although a high accuracy for describing the propagation environments can be achieved by this kind of modeling solution, the high cost and time-consuming feature limit their extension to other communication systems, especially UAV-to-ground communication. By contrast, the latter ones are developed by modeling channel fading characteristics as a stochastic variable, which can endow the channel models with desirable generality. That is, the stochastic channel models can be applied to a variety of communication scenarios by appropriate adjustment of model

parameters [4]. So far, there have been many studies on the modeling of stochastic channels for UAV-to-ground communication. For example, according to geometric correlations among UAVs, GRs, and clusters, the authors in [5] and [6] proposed three-dimensional (3D) geometry-based multiple-input multiple-output (MIMO) channel models for characterizing the UAV-to-ground communication scenarios, and investigated the channel propagation characteristics in spatial and temporal domains. In [7] and [8], the authors proposed ellipsoid and semi-spherical models to describe the UAV-to-ground channels, respectively, and modeled the non-line-of-sight (NLoS) propagation rays from the UAV transmitter to GR as one interaction. Recently, RIS has gradually been applied in UAV-to-ground communication systems and realized high-quality communication through passive beamforming [9]. As a result, many researchers attempt to develop effective channel models to characterize the UAV-to-ground communication scenarios assisted by RIS. For example, the authors in [10] proposed a 3D geometry-based channel model for MIMO communication scenarios assisted by RIS, and investigated the influences of the velocity/direction/motion time of the UAV on the channel propagation characteristics in spatial domain. The authors in [11] proposed a 3D non-stationary MIMO wideband end-to-end channel model for RIS-assisted UAV-to-ground millimeter-wave communication, and analyzed the influences of the physical properties of RIS and the RIS reflection phase configurations on the channel characteristics. In [12], the authors presented a 3D non-stationary UAV-to-ground communication channel model assisted by RIS, and compared the simulation results of propagation characteristics of the channel models with and without RIS assistance.

Previous research work [13] has revealed that the use of double-RIS in wireless communication systems can lead to a significantly increased achievable rate compared to single-RIS assisted systems. In this context, various studies have been carried out on double-RIS assisted wireless communication systems in recent years [14] proposed a cooperative double-RIS assisted MIMO communication system under LoS propagation channels, and investigated the capacity maximization problem by jointly optimizing the transmit covariance matrices and the passive beamforming matrices of the two cooperative RISs. The authors in [15] optimized the cooperative beamforming gain in a communication system assisted by double-RIS, in which a user was serviced from a single-antenna base station (BS) via a dual-hop propagation path of two distributed RISs near the user and the BS respectively. In [16], the authors presented a double-RIS cooperatively-assisted MIMO communication system, where two distributed RISs are respectively deployed near a nearby user group and a multi-antenna BS. The authors in [17] presented a double-RIS assisted MIMO communication system, and the simulation results confirmed the improved performance of the system assisted by double-RIS compared to that by single-RIS under various system settings. Nevertheless, there are only few research results on the channel modeling of double-RIS cooperatively assisted communication systems, which may lead to an underestimation or overestimation of the performance of double-RIS assisted UAV-to-ground communication systems. In addition, the waves emitted from the UAV may undergo different propagation links with different path loss before arriving at the receiver, so the power scaling factors for different propagation links should be derived to capture the fading characteristics of double-RIS assisted UAV-to-ground channels. In this paper, we propose a 3D physics-based end-to-end channel model for double-RIS assisted UAV-to-ground communication with a blocking LoS link operated at sub-6 GHz band, as illustrated in Fig. 1. The main contributions of our work are summarized as follows:

- We propose a 3D physics-based end-to-end MIMO channel model for double-RIS assisted UAV-to-ground propagation environments. The proposed channel model is capable of characterizing both the large-scale path loss and small-scale multi-path effects of UAV-to-ground channels. By properly adjusting model parameters, the proposed channel model can characterize the underlying propagation properties of double-RIS assisted UAV-to-ground channels under different system setups.
- We deduce the complex channel impulse responses (CIRs) for the proposed channel model considering different propagation links, including UAV $\rightarrow$ RIS_1 $\rightarrow$ GR link, UAV $\rightarrow$ RIS_2 $\rightarrow$ GR link, UAV $\rightarrow$ RIS_1 $\rightarrow$ RIS_2 $\rightarrow$ GR link, and UAV $\rightarrow$ clusters $\rightarrow$ GR link. For each distinguishable propagation link, the complex CIR has the ability to characterize the large-scale path loss of the double-RIS assisted UAV-to-ground communication systems.
- We derive the path power gains of different propagation links to characterize the large-scale path loss of the proposed double-RIS assisted UAV-to-ground channel model. Based on the derived path power gains, we introduce the virtual Rice factor to characterize the impact of the configurations of RIS reflection phase on the fading characteristics of the proposed channel model.
- The statistical properties of the proposed double-RIS assisted UAV-to-ground channel model, including spatial cross-correlation functions (CCFs), temporal auto-correlation functions (ACFs), and frequency correlation functions (FCFs), are derived and analyzed. The results show that the reflection phase configurations of RISs, including the optimal and random phase modulations, play important roles in the proposed channel propagation characteristics. This finding can be helpful for the design of double-RIS assisted UAV-to-ground communication systems.

The rest of this paper is organized as follows. Section II deduces the complex CIRs for various propagation links in the proposed channel model. In Section III, the propagation properties of the proposed channel model are deduced and examined. In Section IV, we present the simulation findings and some related discussion. Finally, some conclusions are drawn in Section V.

Notations The boldface uppercase, boldface lowercase, and lowercase letters such as $\mathbf{X}$, $\mathbf{x}$, and x represent the matrix, vector, and scalar, respectively. $\mathbb{E}[\cdot]$ represents the expectation

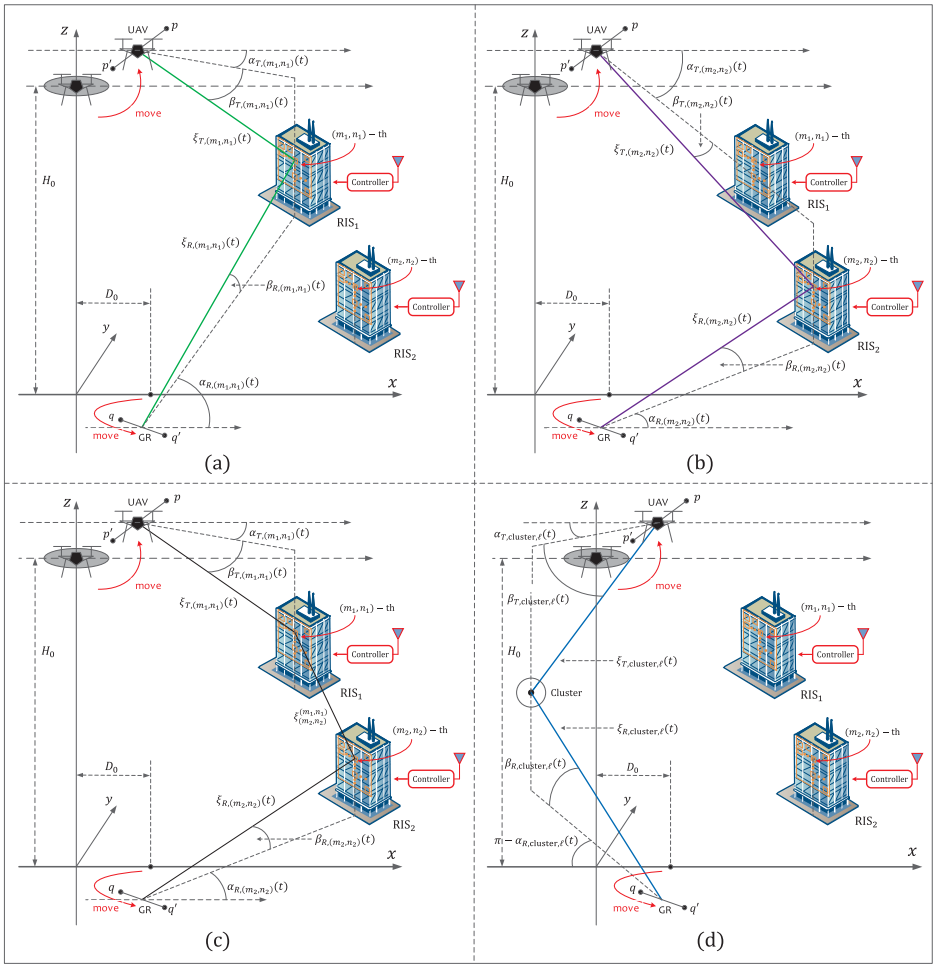

Fig. 1. Propagation distances and angles in the proposed double-RIS assisted UAV-to-ground channel model for different links. (a) UAV → RIS_1 → GR link; (b) UAV → RIS_2 → GR link; (c) UAV → RIS_1 → RIS_2 → GR link; (d) UAV → clusters → GR link.

operation, $[\cdot]^{\text{T}}$ represents the transpose operation, and $(\cdot)^*$ represents the complex conjugate operation. $\|\cdot\|$ is the Frobenius norm, and $j = \sqrt{-1}$ denotes the imaginary unit.

II. System Channel Model Description

In UAV-to-GR wireless channels, the LoS propagation link between UAV and GR is not always blocked because of the dynamic properties of the transceivers. In reality, it experiences blockage occasionally with the motion of the UAV and GR [18]. Current studies have shown that when the LoS component between the UAV and GR is heavily blocked by objects such as buildings, an RIS can be employed to provide a strong LoS link from UAV to RIS and from RIS to GR, thus boosting the communication performance [11]. Owing to the manipulation of the RIS array on the amplitude and/or the phase of incident signals, the wireless propagation environment between the RIS and GR is programmable. Specifically, the impinging wave can be restricted in a desired direction with a certain beamwidth in the RIS-GR subchannel. This means that some unnecessary propagation links that may cause poor communication performance, such as the RIS → clusters → GR link, can be avoided in the propagation environment between the RIS and GR in RIS-assisted channels.

TABLE I
Definitions of Key Parameters

δ_T, δ_R	Spacings between two neighboring UAV/GR antennas
ψ_T, ϕ_T	Azimuth and elevation angles of the UAV antenna array
ψ_R, ϕ_R	Azimuth and elevation angles of the GR antenna array
D_0, H_0	Distances from the center of UAV antenna array to that of GR antenna array and to the azimuth plane
v_R, γ_R	Moving speed and azimuth direction of the GR
M_1, N_1	Numbers of arranged cells of RIS_1 array in the horizontal and vertical directions
M_2, N_2	Numbers of arranged cells of RIS_2 array in the horizontal and vertical directions
d_{M_1}, d_{N_1}	Sizes of each unit in RIS_1 along the horizontal and vertical directions
d_{M_2}, d_{N_2}	Sizes of each unit in RIS_2 along the horizontal and vertical directions

Fig. 1 illustrates a 3D physics-based end-to-end double-RIS assisted channel model for UAV-to-ground propagation environments, where the RIS near the UAV transmitter is named RIS_1 and the other near the GR is named RIS_2. Each RIS is equipped with a controller that can identify the phase offset of reflective elements on each RIS [19]. In the initial motion stage of the UAV and GR, a global Cartesian coordinate system is created. To be specific, the line connecting the

center of GR antenna array with the projection point of UAV antenna array is defined as the x-axis, the z-axis is vertical up and passes through the center of UAV antenna array, and the y-axis is obtained in accordance with right-hand rule [20]. The definitions of the key model parameters are depicted in Fig. 1 and summarized in Table I. It is worth noting that the suggested coordinate system is still maintained even when the UAV and GR move from one position to another. As a result, the distance vectors from the origin of the global coordinate system to the centroids of the UAV and GR antenna arrays can be represented by $\mathbf{d}_T(t) = [\, d_{T,x}(t), d_{T,y}(t), d_{T,z}(t)\,]^{\mathrm{T}}$ and $\mathbf{d}_R(t) = [\, d_{R,x}(t), d_{R,y}(t), 0\,]^{\mathrm{T}}$ respectively, where $d_{T,x}(t) = v_T t \cos\gamma_T \cos\eta_T$, $d_{T,y}(t) = v_T t \cos\gamma_T \sin\eta_T$, $d_{T,z}(t) = H_0 + v_T t \sin\gamma_T$, $d_{R,x}(t) = D_0 + v_R t \cos\eta_R$, and $d_{R,y}(t) = v_R t \sin\eta_T$. In the proposed channel model, the UAV and GR are respectively composed of P and Q omnidirectional antennas in a uniform linear array (ULA). Distance vectors from the p-th ($p = 1, 2, \ldots, P$) UAV antenna to the q-th ($q = 1, 2, \ldots, Q$) GR antenna to the origin of the global coordinate system can be respectively described as

$$\mathbf{Ant}_p = \frac{P - 2p + 1}{2}\delta_T \begin{bmatrix} \cos\phi_T \cos\psi_T \\ \cos\phi_T \sin\psi_T \\ \sin\phi_T \end{bmatrix}, \tag{1}$$

$$\mathbf{Ant}_q = \frac{Q - 2q + 1}{2}\delta_R \begin{bmatrix} \cos\phi_R \cos\psi_R \\ \cos\phi_R \sin\psi_R \\ \sin\phi_R \end{bmatrix}. \tag{2}$$

The distance vectors from the origin of the global coordinate system to the center points of RIS_1 and RIS_2 are $\mathbf{d}_{\mathrm{RIS}_1} = [\, x_{\mathrm{RIS}_1}, y_{\mathrm{RIS}_1}, z_{\mathrm{RIS}_1}\,]^{\mathrm{T}}$ and $\mathbf{d}_{\mathrm{RIS}_2} = [\, x_{\mathrm{RIS}_2}, y_{\mathrm{RIS}_2}, z_{\mathrm{RIS}_2}\,]^{\mathrm{T}}$, respectively. Thus, the distance from the center of RIS_1 to that of RIS_2 can be derived by $\xi_{\mathrm{RIS}_2}^{\mathrm{RIS}_1} = \| \mathbf{d}_{\mathrm{RIS}_1} - \mathbf{d}_{\mathrm{RIS}_2} \|$. The distance vector from the origin of the global coordinate system to the cluster is denoted by $\mathbf{d}_{\mathrm{cluster}} = [\, x_{\mathrm{cluster}}, y_{\mathrm{cluster}}, z_{\mathrm{cluster}}\,]^{\mathrm{T}}$. In order to strengthen the generality of the double-RIS layout in the proposed channel model, θ_{RIS_1} and θ_{RIS_2} are introduced to describe the practical horizontal rotation angles of RIS_1 and RIS_2, respectively [21]. Then, the distance vectors from the origin of the global coordinate system to the (m_1, n_1)-th ($m_1 = 1, 2, \ldots M_1; n_1 = 1, 2, \ldots N_1$) unit in RIS_1 and the (m_2, n_2)-th ($m_2 = 1, 2, \ldots M_2; n_2 = 1, 2, \ldots N_2$) unit in RIS_2 can be respectively expressed as

$$\begin{aligned} \mathbf{d}_{m_1,n_1} &= \begin{bmatrix} x_{m_1,n_1} \\ y_{m_1,n_1} \\ z_{m_1,n_1} \end{bmatrix} \\ &= \begin{bmatrix} x_{\mathrm{RIS}_1} + \frac{1}{2}(2\ m_1 - M_1 - 1) d_{M_1} \cos\theta_{\mathrm{RIS}_1} \\ y_{\mathrm{RIS}_1} + \frac{1}{2}(2\ m_1 - M_1 - 1) d_{M_1} \sin\theta_{\mathrm{RIS}_1} \\ z_{\mathrm{RIS}_1} - \frac{1}{2}(2\ n_1 - N_1 - 1) d_{N_1} \end{bmatrix}, \\ \mathbf{d}_{m_2,n_2} &= \begin{bmatrix} x_{m_2,n_2} \\ y_{m_2,n_2} \\ z_{m_2,n_2} \end{bmatrix} \\ &= \begin{bmatrix} x_{\mathrm{RIS}_2} + \frac{1}{2}(2\ m_2 - M_2 - 1) d_{M_2} \cos\theta_{\mathrm{RIS}_2} \\ y_{\mathrm{RIS}_2} + \frac{1}{2}(2\ m_2 - M_2 - 1) d_{M_2} \sin\theta_{\mathrm{RIS}_2} \\ z_{\mathrm{RIS}_2} - \frac{1}{2}(2\ n_2 - N_2 - 1) d_{N_2} \end{bmatrix}. \end{aligned} \tag{3, 4}$$

A. Complex CIRs of the Proposed Channel Model

In the proposed double-RIS assisted UAV-to-ground MIMO channel model, the movements of the UAV and GR will cause time-varying model parameters, including propagation distances and angles, resulting in the temporal non-stationary property of the channel. In light of this, time-varying model parameters, including time-varying propagation distances and angles, are required to be derived to capture the non-stationary channel propagation characteristics in time domain. As shown in Fig. 1, the wave emitted by the UAV goes through four different propagation paths before arriving at the GR, which constitute the multi-path propagations of the proposed channel model. Namely, i) the waves impinges on RIS_1 before arriving at the GR, i.e., UAV $\rightarrow$ RIS_1 $\rightarrow$ GR link; ii) the wave impinges on RIS_2 before arriving at the GR, i.e., UAV $\rightarrow$ RIS_2 $\rightarrow$ GR link; iii) the wave impinges on RIS_1 first and then on RIS_2 before arriving at the GR, i.e., UAV $\rightarrow$ RIS_1 $\rightarrow$ RIS_2 $\rightarrow$ GR link; iv) the wave impinges on the cluster before arriving at the GR, i.e., UAV $\rightarrow$ clusters $\rightarrow$ GR link. In consideration of both large-scale path loss and small-scale multi-path fading, the complete end-to-end channel matrix between the UAV and GR can be written as [22]

$$\mathbf{H}_{\mathrm{TR}}(t) = \sqrt{\Omega_{\mathrm{TR}}^{\mathrm{large}}(t)} \cdot \mathbf{H}_{\mathrm{TR}}^{\mathrm{small}}(t), \tag{5}$$

where $\Omega_{\mathrm{TR}}^{\mathrm{large}}(t)$ represents the path power gain, and the matrix $\mathbf{H}_{\mathrm{TR}}^{\mathrm{small}}(t)$ denotes the small-scale fading between different transmit-receive antenna pairs in the proposed channel model. In this case, its path loss can be characterized by $1/\Omega_{\mathrm{TR}}^{\mathrm{large}}(t)$. Although 3GPP gives the UAV-to-ground path loss model for different frequency bands and scenarios [23], it fails to characterize the path loss in RIS-assisted UAV-to-ground channels. In the proposed channel model, the overall path power gain can be described as $\Omega_{\mathrm{TR}}^{\mathrm{large}}(t) = \Omega_{\mathrm{TR}}^{\mathrm{RIS}_1}(t) + \Omega_{\mathrm{TR}}^{\mathrm{RIS}_2}(t) + \Omega_{\mathrm{TR}}^{\mathrm{RIS}_{12}}(t) + \Omega_{\mathrm{TR}}^{\mathrm{cluster}}(t)$, where $\Omega_{\mathrm{TR}}^{\mathrm{RIS}_1}(t)$, $\Omega_{\mathrm{TR}}^{\mathrm{RIS}_2}(t)$, $\Omega_{\mathrm{TR}}^{\mathrm{RIS}_{12}}(t)$, and $\Omega_{\mathrm{TR}}^{\mathrm{cluster}}(t)$ represent the link power gains of the UAV $\rightarrow$ RIS_1 $\rightarrow$ GR link, UAV $\rightarrow$ RIS_2 $\rightarrow$ GR link, UAV $\rightarrow$ RIS_1 $\rightarrow$ RIS_2 $\rightarrow$ GR link, and UAV $\rightarrow$ clusters $\rightarrow$ GR link, respectively. Their derivations can be found in Appendix. The small-scale fading is caused by multi-path propagation components, which can be denoted by a $Q \times P$ complex matrix, i.e., $\mathbf{H}_{\mathrm{TR}}^{\mathrm{small}}(t) = \big[h_{pq}(t,\tau)\big]_{Q\times P}$. Here, $h_{pq}(t,\tau)$ stands for the complex CIR between the p-th UAV antenna and the q-th GR antenna of the proposed MIMO channel model, which can be described as

$$\begin{aligned} h_{pq}(t,\tau) = &\sqrt{\frac{\Omega_{\mathrm{TR}}^{\mathrm{RIS}_1}(t)}{\Omega_{\mathrm{TR}}^{\mathrm{large}}(t)}} h_{pq}^{\mathrm{RIS}_1}(t)\delta\big(\tau - \tau^{\mathrm{RIS}_1}(t)\big) \\ &+ \sqrt{\frac{\Omega_{\mathrm{TR}}^{\mathrm{RIS}_2}(t)}{\Omega_{\mathrm{TR}}^{\mathrm{large}}(t)}} h_{pq}^{\mathrm{RIS}_2}(t)\delta\big(\tau - \tau^{\mathrm{RIS}_2}(t)\big) \end{aligned}$$

$$+\sqrt{\frac{\Omega_{\mathrm{TR}}^{\mathrm{RIS}_{12}}(t)}{\Omega_{\mathrm{TR}}^{\mathrm{large}}(t)}}h_{pq}^{\mathrm{RIS}_{12}}(t)\delta\big(\tau-\tau^{\mathrm{RIS}_{12}}(t)\big)$$
$$+\sqrt{\frac{\Omega_{\mathrm{TR}}^{\mathrm{cluster}}(t)}{\Omega_{\mathrm{TR}}^{\mathrm{large}}(t)}}h_{pq}^{\mathrm{cluster}}(t)\delta\big(\tau-\tau^{\mathrm{cluster}}(t)\big), \quad (6)$$

where $\tau^{\mathrm{RIS}_1}(t) = \big(\xi_{T,\mathrm{RIS}_1}(t)+\xi_{T,\mathrm{RIS}_1}(t)\big)/c$, in which $\xi_{T,\mathrm{RIS}_1}(t) = \|\mathbf{d}_{\mathrm{RIS}_1}-\mathbf{d}_T(t)\|$ and $\xi_{R,\mathrm{RIS}_1}(t) = \|\mathbf{d}_{\mathrm{RIS}_1}-\mathbf{d}_R(t)\|$ represent the time-varying distances from the centers of UAV and GR antenna arrays to that of RIS_1 array respectively, and c is the light speed; $\tau^{\mathrm{RIS}_2}(t) = \big(\xi_{T,\mathrm{RIS}_2}(t)+\xi_{R,\mathrm{RIS}_2}(t)\big)/c$, in which $\xi_{T,\mathrm{RIS}_2}(t) = \|\mathbf{d}_{\mathrm{RIS}_2}-\mathbf{d}_T(t)\|$ and $\xi_{R,\mathrm{RIS}_2}(t) = \|\mathbf{d}_{\mathrm{RIS}_2}-\mathbf{d}_R(t)\|$ represent the time-varying distances from the centers of UAV and GR antenna arrays to that of RIS_2 array respectively; $\tau^{\mathrm{RIS}_{12}}(t) = \big(\xi_{T,\mathrm{RIS}_1}(t)+\xi_{\mathrm{RIS}_2}^{\mathrm{RIS}_1}+\xi_{R,\mathrm{RIS}_2}(t)\big)/c$ and $\tau^{\mathrm{cluster}}(t) = \big(\xi_{T,\mathrm{cluster}}(t)+\xi_{R,\mathrm{cluster}}(t)\big)/c$, in which $\xi_{T,\mathrm{cluster}}(t) = \|\mathbf{d}_{\mathrm{cluster}}-\mathbf{d}_T(t)\|$ and $\xi_{R,\mathrm{cluster}}(t) = \|\mathbf{d}_{\mathrm{cluster}}-\mathbf{d}_R(t)\|$ represent the time-varying distances from the centers of UAV and GR antenna arrays to the center of the cluster in the real-time motion stage respectively.

For the UAV $\rightarrow$ RIS_1 $\rightarrow$ GR propagation link, the channel coefficient $h_{pq}^{\mathrm{RIS}_1}(t)$ for the (p,q)-th antenna pair can be expressed as [11]

$$\begin{aligned}h_{pq}^{\mathrm{RIS}_1}(t) = \sqrt{\frac{1}{\Upsilon_{pq}^{\mathrm{RIS}_1}(t)}}\sum_{m_1=1}^{M_1}\sum_{n_1=1}^{N_1}\chi_{m_1,n_1}(t)e^{j\varphi_{m_1,n_1}(t)}\\ \times e^{-j\frac{2\pi}{\lambda}\left(\xi_{p,(m_1,n_1)}(t)+\xi_{q,(m_1,n_1)}(t)\right)}\\ \times e^{j\frac{2\pi}{\lambda}v_Tt\cos\left(\alpha_{T,(m_1,n_1)}(t)-\eta_T\right)\cos\beta_{T,(m_1,n_1)}(t)\cos\gamma_T}\\ \times e^{j\frac{2\pi}{\lambda}v_Tt\sin\beta_{T,(m_1,n_1)}(t)\sin\gamma_T}\\ \times e^{j\frac{2\pi}{\lambda}v_Rt\cos\left(\alpha_{R,(m_1,n_1)}(t)-\eta_R\right)\cos\beta_{R,(m_1,n_1)}(t)},\end{aligned} \quad (7)$$

where λ is the wavelength; $\varphi_{m_1,n_1}(t)$ and $\chi_{m_1,n_1}(t)$ represent the reflection phase and amplitude of the (m_1,n_1)-th unit in RIS_1, respectively; $\Upsilon_{pq}^{\mathrm{RIS}_1}(t)$ is the normalized factor of the UAV $\rightarrow$ RIS_1 $\rightarrow$ GR link to endow $h_{pq}^{\mathrm{RIS}_1}(t)$ with unit power; $\xi_{p,(m_1,n_1)}(t)$ and $\xi_{q,(m_1,n_1)}(t)$ respectively stand for the lengths from the p-th UAV and the q-th GR antenna to the (m_1,n_1)-th unit in RIS_1, i.e., $\xi_{p,(m_1,n_1)}(t) = \|\mathbf{d}_{m_1,n_1}-\mathbf{d}_T(t)-\mathbf{Ant}_p\|$ and $\xi_{q,(m_1,n_1)}(t) = \|\mathbf{d}_{m_1,n_1}-\mathbf{d}_R(t)-\mathbf{Ant}_q\|$. When RIS_1 adopts the uniform reflection phase configuration, it is reasonable to assume that $\varphi_{m_1,n_1}(t)$ follows the uniform distribution. However, when the phase regulation is discrete, $\varphi_{m_1,n_1}(t)$ should be set to be some discrete values. $\Upsilon_{pq}^{\mathrm{RIS}_1}(t)$ can be expressed as

$$\begin{aligned}&\Upsilon_{pq}^{\mathrm{RIS}_1}(t)\\ &= \mathbb{E}\Big\{\Big|\sum_{m_1=1}^{M_1}\sum_{n_1=1}^{N_1}\chi_{m_1,n_1}(t)e^{j\varphi_{m_1,n_1}(t)}\\ &\quad\times e^{-j\frac{2\pi}{\lambda}\left(\xi_{p,(m_1,n_1)}(t)+\xi_{q,(m_1,n_1)}(t)\right)}\\ &\quad\times e^{j\frac{2\pi}{\lambda}v_Tt\cos\left(\alpha_{T,(m_1,n_1)}(t)-\eta_T\right)\cos\beta_{T,(m_1,n_1)}(t)\cos\gamma_T}\\ &\quad\times e^{j\frac{2\pi}{\lambda}v_Tt\sin\beta_{T,(m_1,n_1)}(t)\sin\gamma_T}\\ &\quad\times e^{j\frac{2\pi}{\lambda}v_Rt\cos\left(\alpha_{R,(m_1,n_1)}(t)-\eta_R\right)\cos\beta_{R,(m_1,n_1)}(t)}\Big|^2\Big\}.\end{aligned} \quad (8)$$

It is necessary to mention that the initial delay/angle/distance parameters can be identified once the geometric settings among UAV, RIS_1, and GR are provided. The geometric correlations among UAV, RIS_1, and GR can be used to obtain the values of model parameters after a time interval of t in accordance with the motion time/direction/velocity, as well as the values of values of initial parameters of UAV and GR [24]. Since we adopt the near-field assumption to investigate the proposed channel characteristics, the RIS units share different signal angles. In light of this, the AAoD and EAoD from the UAV to the (m_1,n_1)-th unit in RIS_1 can be respectively represented as

$$\begin{aligned}&\alpha_{T,(m_1,n_1)}(t)\\ &= \arctan\frac{y_{m_1,n_1}-d_{T,y}(t)}{x_{m_1,n_1}-d_{T,x}(t)},\end{aligned} \quad (9)$$

$$\begin{aligned}&\beta_{T,(m_1,n_1)}(t)\\ &= \arctan\frac{z_{m_1,n_1}-d_{T,z}(t)}{\sqrt{\big(x_{m_1,n_1}-d_{T,x}(t)\big)^2+\big(y_{m_1,n_1}-d_{T,y}(t)\big)^2}}.\end{aligned} \quad (10)$$

The AAoA and EAoA from the (m_1,n_1)-th unit in RIS_1 to the GR can be respectively expressed as

$$\begin{aligned}&\alpha_{R,(m_1,n_1)}(t)\\ &= \arctan\frac{y_{m_1,n_1}-d_{R,y}(t)}{x_{m_1,n_1}-d_{R,x}(t)},\end{aligned} \quad (11)$$

$$\begin{aligned}&\beta_{R,(m_1,n_1)}(t)\\ &= \arctan\frac{z_{m_1,n_1}}{\sqrt{\big(x_{m_1,n_1}-d_{R,x}(t)\big)^2+\big(y_{m_1,n_1}-d_{R,y}(t)\big)^2}}.\end{aligned} \quad (12)$$

For the UAV $\rightarrow$ RIS_2 $\rightarrow$ GR propagation link, the channel coefficient $h_{pq}^{\mathrm{RIS}_2}(t)$ for the (p,q)-th antenna pair can be written as

$$\begin{aligned}h_{pq}^{\mathrm{RIS}_2}(t) = \sqrt{\frac{1}{\Upsilon_{pq}^{\mathrm{RIS}_2}(t)}}\sum_{m_2=1}^{M_2}\sum_{n_2=1}^{N_2}\chi_{m_2,n_2}(t)e^{j\varphi_{m_2,n_2}(t)}\\ \times e^{-\frac{2\pi}{\lambda}\left(\xi_{p,(m_2,n_2)}(t)+\xi_{q,(m_2,n_2)}(t)\right)}\\ \times e^{j\frac{2\pi}{\lambda}v_Tt\cos\left(\alpha_{T,(m_2,n_2)}(t)-\eta_T\right)\cos\beta_{T,(m_2,n_2)}(t)\cos\gamma_T}\\ \times e^{j\frac{2\pi}{\lambda}v_Tt\sin\beta_{T,(m_2,n_2)}(t)\sin\gamma_T}\\ \times e^{j\frac{2\pi}{\lambda}v_Rt\cos\left(\alpha_{R,(m_2,n_2)}(t)-\eta_R\right)\cos\beta_{R,(m_2,n_2)}(t)},\end{aligned} \quad (13)$$

where $\varphi_{m_2,n_2}(t)$ and $\chi_{m_2,n_2}(t)$ represent the reflection phase and amplitude of the (m_2,n_2)-th unit in RIS_2, respectively; $\Upsilon_{pq}^{\mathrm{RIS}_2}(t)$ is the normalized factor of the UAV $\rightarrow$ RIS_2 $\rightarrow$ GR link, which can be expressed as

$$\begin{aligned}&\Upsilon_{pq}^{\mathrm{RIS}_2}(t)\\ &= \mathbb{E}\Big\{\Big|\sum_{m_2=1}^{M_2}\sum_{n_2=1}^{N_2}\chi_{m_2,n_2}(t)e^{j\varphi_{m_2,n_2}(t)}\\ &\quad\times e^{-j\frac{2\pi}{\lambda}\left(\xi_{p,(m_2,n_2)}(t)+\xi_{q,(m_2,n_2)}(t)\right)}\\ &\quad\times e^{j\frac{2\pi}{\lambda}v_Tt\cos\left(\alpha_{T,(m_2,n_2)}(t)-\eta_T\right)\cos\beta_{T,(m_2,n_2)}(t)\cos\gamma_T}\end{aligned}$$

$$\times e^{j\frac{2\pi}{\lambda}v_T t\sin\beta_{T,(m_2,n_2)}(t)\sin\gamma_T} \times e^{j\frac{2\pi}{\lambda}v_R t\cos\left(\alpha_{R,(m_2,n_2)}(t)-\eta_R\right)\cos\beta_{R,(m_2,n_2)}(t)}\Big|^2\Big\}. \quad (14)$$

It is important to mention that the process of deriving the model parameters for the UAV $\rightarrow$ RIS$_2$ $\rightarrow$ GR link is the same as that for the UAV $\rightarrow$ RIS$_1$ $\rightarrow$ GR link. By replacing all the subscripts $[\cdot]_1$ in Eqs. (9)-(12) with $[\cdot]_2$, the corresponding time-varying distances/angles for the RIS$_2$ propagation link can be obtained. Here, we omit them for brevity.

For the UAV $\rightarrow$ RIS$_1$ $\rightarrow$ RIS$_2$ $\rightarrow$ GR propagation link, the channel coefficient $h_{pq}^{\text{RIS}_{12}}(t)$ can be written as

$$\begin{aligned} h_{pq}^{\text{RIS}_{12}}(t) &= \sqrt{\frac{1}{\Upsilon_{pq}^{\text{RIS}_{12}}(t)}}\sum_{m_2=1}^{M_2}\sum_{n_2=1}^{N_2}\sum_{m_1=1}^{M_1}\sum_{n_1=1}^{N_1}\chi_{m_1,n_1}(t)\chi_{m_2,n_2}(t) \\ &\times e^{j\left(\varphi_{m_1,n_1}(t)+\varphi_{m_2,n_2}(t)\right)} \\ &\times e^{-j\frac{2\pi}{\lambda}\left(\xi_{T,(m_1,n_1)}(t)+\xi_{(m_2,n_2)}^{(m_1,n_1)}+\xi_{R,(m_2,n_2)}(t)\right)} \\ &\times e^{j\frac{2\pi}{\lambda}v_T t\cos\left(\alpha_{T,(m_1,n_1)}(t)-\eta_T\right)\cos\beta_{T,(m_1,n_1)}(t)\cos\gamma_T} \\ &\times e^{j\frac{2\pi}{\lambda}v_T t\sin\beta_{T,(m_1,n_1)}(t)\sin\gamma_T} \\ &\times e^{j\frac{2\pi}{\lambda}v_R t\cos\left(\alpha_{R,(m_2,n_2)}(t)-\eta_R\right)\cos\beta_{R,(m_2,n_2)}(t)}, \end{aligned} \quad (15)$$

where $\xi_{(m_2,n_2)}^{(m_1,n_1)} = \|\mathbf{d}_{m_1,n_1} - \mathbf{d}_{m_2,n_2}\|$ represents the distance from the (m_1,n_1)-th unit in RIS$_1$ to the (m_2,n_2)-th unit in RIS$_2$; $\Upsilon_{pq}^{\text{RIS}_{12}}(t)$ is the normalized factor of the UAV $\rightarrow$ RIS$_1$ $\rightarrow$ RIS$_2$ $\rightarrow$ GR link, which can be expressed as

$$\begin{aligned} \Upsilon_{pq}^{\text{RIS}_{12}}(t) &= \mathbb{E}\Big\{\Big|\sum_{m_2=1}^{M_2}\sum_{n_2=1}^{N_2}\sum_{m_1=1}^{M_1}\sum_{n_1=1}^{N_1}\chi_{m_1,n_1}\chi_{m_2,n_2}(t) \\ &\times e^{j\left(\varphi_{m_1,n_1}(t)+\varphi_{m_2,n_2}(t)\right)} \\ &\times e^{-j\frac{2\pi}{\lambda}\left(\xi_{p,(m_1,n_1)}(t)+\xi_{(m_2,n_2)}^{(m_1,n_1)}+\xi_{q,(m_2,n_2)}(t)\right)} \\ &\times e^{j\frac{2\pi}{\lambda}v_T t\cos\left(\alpha_{T,(m_1,n_1)}(t)-\eta_T\right)\cos\beta_{T,(m_1,n_1)}(t)\cos\gamma_T} \\ &\times e^{j\frac{2\pi}{\lambda}v_T t\sin\beta_{T,(m_1,n_1)}(t)\sin\gamma_T} \\ &\times e^{j\frac{2\pi}{\lambda}v_R t\cos\left(\alpha_{R,(m_2,n_2)}(t)-\eta_R\right)\cos\beta_{R,(m_2,n_2)}(t)}\Big|^2\Big\}. \end{aligned} \quad (16)$$

For the NLoS propagation link via the cluster, the channel coefficient $h_{pq}^{\text{cluster}}(t)$ can be described as

$$\begin{aligned} h_{pq}^{\text{cluster}}(t) = \frac{1}{\sqrt{L}}\sum_{\ell=1}^{L} & e^{j\left(\varphi_\ell-\frac{2\pi}{\lambda}\left(\xi_{p,\text{cluster},\ell}(t)+\xi_{q,\text{cluster},\ell}(t)\right)\right)} \\ &\times e^{j\frac{2\pi}{\lambda}v_T t\cos\left(\alpha_{T,\text{cluster},\ell}(t)-\eta_T\right)\cos\beta_{T,\text{cluster},\ell}(t)\cos\gamma_T} \\ &\times e^{j\frac{2\pi}{\lambda}v_T t\sin\beta_{T,\text{cluster},\ell}(t)\sin\gamma_T} \\ &\times e^{j\frac{2\pi}{\lambda}v_R t\cos\left(\alpha_{R,\text{cluster},\ell}(t)-\eta_R\right)\cos\beta_{R,\text{cluster},\ell}(t)}. \end{aligned} \quad (17)$$

Here, L denotes the numbers of NLoS rays within the cluster, which is typically presumed to be close to infinity, i.e., $L \rightarrow \infty$; $\{\varphi_\ell\}_{\ell=1,2,\ldots L}$ is presumed to be a uniformly and independently distributed random phase, i.e., $\varphi_\ell \sim \text{U}[-\pi,\pi)$. The initial delay/angle/distance parameters are derived from the randomly generated or measured activity. Scatterers in the same cluster are presumed to have roughly the same initial separation from the center of GR antenna array at different angles, i.e., $\xi_{R,\text{cluster}}(0) \approx \xi_{R,\text{cluster},1}(0)\cdots \approx \xi_{R,\text{cluster},\ell}(0)\cdots \approx \xi_{R,\text{cluster},L}(0)$ [25]. Subsequently, the time-varying distances from the p-th UAV antenna and the q-th GR antenna to the ℓ-th scatterer within the cluster can be respectively determined through taking the magnitudes of $\xi_{p,\text{cluster},\ell}(t) = \|\mathbf{d}_{p,\text{cluster},\ell}(t)\|$ and $\xi_{q,\text{cluster},\ell}(t) = \|\mathbf{d}_{q,\text{cluster},\ell}(t)\|$, i.e.,

$$\mathbf{d}_{p,\text{cluster},\ell}(t) = \begin{bmatrix} g_{1x}-d_{T,x}(t) \\ g_{1y}-d_{T,y}(t) \\ g_{1z}-d_{T,z}(t)\end{bmatrix} - \mathbf{Ant}_p, \quad (18)$$

$$\mathbf{d}_{q,\text{cluster},\ell}(t) = \begin{bmatrix} g_{2x}-d_{R,x}(t) \\ g_{2y}-d_{R,y}(t) \\ g_{2z}\end{bmatrix} - \mathbf{Ant}_q, \quad (19)$$

where $g_{1x} = \xi_{T,\text{cluster}}(0)\cos\beta_{T,\text{cluster},\ell}(0)\cos\alpha_{T,\text{cluster},\ell}(0)$, $g_{1y} = \xi_{T,\text{cluster}}(0)\cos\beta_{T,\text{cluster},\ell}(0)\sin\alpha_{T,\text{cluster},\ell}(0)$, and $g_{1z} = \xi_{T,\text{cluster}}(0)\sin\beta_{T,\text{cluster},\ell}(0)$, respectively; and $g_{2x} = \xi_{R,\text{cluster}}(0)\cos\beta_{R,\text{cluster},\ell}(0)\cos\alpha_{R,\text{cluster},\ell}(0)$, $g_{2y} = \xi_{R,\text{cluster}}(0)\cos\beta_{R,\text{cluster},\ell}(0)\sin\alpha_{R,\text{cluster},\ell}(0)$, and $g_{2z} = \xi_{R,\text{cluster}}(0)\sin\beta_{R,\text{cluster},\ell}(0)$, respectively. The $\xi_{T,\text{cluster}}(0)$ and $\xi_{R,\text{cluster}}(0)$ are respectively the distances from the centers of the UAV and GR antenna arrays to that of the cluster in initial motion stage, i.e., $t=0$; $\alpha_{T,\text{cluster},\ell}(0)$ and $\beta_{T,\text{cluster},\ell}(0)$ are respectively the AAoD and EAoD of the wave impinging on the ℓ-th scatterer within the cluster from the UAV in the initial motion stage; $\alpha_{R,\text{cluster},\ell}(0)$ and $\beta_{R,\text{cluster},\ell}(0)$ are respectively the AAoA and EAoA of the wave scattered from the cluster. Moreover, the time-varying EAoD and AAoD of the wave from the UAV to the ℓ-th scatterer within the cluster can be respectively represented as

$$\alpha_{T,\text{cluster},\ell}(t) = \arctan\frac{g_{1y}-d_{T,y}(t)}{g_{1x}-d_{T,x}(t)}, \quad (20)$$

$$\beta_{T,\text{cluster},\ell}(t) = \text{arccot}\frac{\sqrt{(g_{1x}-d_{T,x}(t))^2+(g_{1y}-d_{T,y}(t))^2}}{g_{1z}-d_{T,z}(t)}. \quad (21)$$

In addition, the time-varying AAoA and EAoA of the wave from the ℓ-th scatterer to GR can be respectively described as

$$\alpha_{R,\text{cluster},\ell}(t) = \arctan\frac{g_{2y}-d_{R,y}(t)}{g_{2x}-d_{R,x}(t)}, \quad (22)$$

$$\beta_{R,\text{cluster},\ell}(t) = \text{arccot}\frac{\sqrt{(g_{2x}-d_{R,x}(t))^2+(g_{2y}-d_{R,y}(t))^2}}{\xi_{R,\text{cluster}}(0)\sin\beta_{R,\text{cluster},\ell}(0)}. \quad (23)$$

B. Virtual Rice Factor

When there is a LoS propagation path between UAV and GR, it provides a deterministic component resulting in the Rician fading for underlying propagation channel. The Rice factor can be defined as the power ratio of the deterministic LoS component to stochastic NLoS component. Through proper programming of RIS reflection phase configuration, the RIS component has the ability of giving a deterministic component to received signals, which also leads to the Rician fading of propagation channels. In this context, we introduce a *virtual Rice factor* $K^{vir}(t)$, which is also defined as the power

ratio of the deterministic component to random component, for characterizing the Rician fading channels in the absence of LoS path [11]. In the proposed double-RIS channel model, the reflection phase configurations of the RISs are separated into following four cases.

Case I: RIS$_1$ and RIS$_2$ both adopt optimal reflection phase configurations. In this case, $h_{pq}^{\mathrm{RIS}_1}(t)$, $h_{pq}^{\mathrm{RIS}_2}(t)$, and $h_{pq}^{\mathrm{RIS}_{12}}(t)$ in Eq. (6) are all deterministic components, while $h_{pq}^{\mathrm{cluster}}(t)$ is a stochastic component. Then, the virtual Rice factor $K^{\mathrm{vir}}(t)$ can be expressed as

$$K^{\mathrm{vir}}(t)=\frac{\Omega_{\mathrm{TR}}^{\mathrm{RIS}_1}(t)+\Omega_{\mathrm{TR}}^{\mathrm{RIS}_2}(t)+\Omega_{\mathrm{TR}}^{\mathrm{RIS}_{12}}(t)}{\Omega_{\mathrm{TR}}^{\mathrm{cluster}}(t)}, \tag{24}$$

and Eq. (6) can be rewritten as follows:

$$\begin{aligned}
&h_{pq}(t,\tau)\\
&=\sqrt{\frac{K^{\mathrm{vir}}(t)}{K^{\mathrm{vir}}(t)+1}}\sqrt{\frac{\Omega_{\mathrm{TR}}^{\mathrm{RIS}_1}(t)}{\Omega_I}}\,h_{pq}^{\mathrm{RIS}_1}(t)\delta\big(\tau-\tau^{\mathrm{RIS}_1}(t)\big)\\
&\quad+\sqrt{\frac{K^{\mathrm{vir}}(t)}{K^{\mathrm{vir}}(t)+1}}\sqrt{\frac{\Omega_{\mathrm{TR}}^{\mathrm{RIS}_2}(t)}{\Omega_I}}\,h_{pq}^{\mathrm{RIS}_2}(t)\delta\big(\tau-\tau^{\mathrm{RIS}_2}(t)\big)\\
&\quad+\sqrt{\frac{K^{\mathrm{vir}}(t)}{K^{\mathrm{vir}}(t)+1}}\sqrt{\frac{\Omega_{\mathrm{TR}}^{\mathrm{RIS}_{12}}(t)}{\Omega_I}}\,h_{pq}^{\mathrm{RIS}_{12}}(t)\delta\big(\tau-\tau^{\mathrm{RIS}_{12}}(t)\big)\\
&\quad+\sqrt{\frac{1}{K^{\mathrm{vir}}(t)+1}}\,h_{pq}^{\mathrm{cluster}}(t)\delta\big(\tau-\tau^{\mathrm{cluster}}(t)\big),
\end{aligned} \tag{25}$$

where $\Omega_I=\Omega_{\mathrm{TR}}^{\mathrm{RIS}_1}(t)+\Omega_{\mathrm{TR}}^{\mathrm{RIS}_2}(t)+\Omega_{\mathrm{TR}}^{\mathrm{RIS}_{12}}(t)$.

Case II: RIS$_1$ adopts the optimal reflection phase configuration while RIS$_2$ adopts a random phase configuration. In this case, $h_{pq}^{\mathrm{RIS}_1}(t)$ is a deterministic component, while $h_{pq}^{\mathrm{RIS}_2}(t)$ and $h_{pq}^{\mathrm{RIS}_{12}}(t)$ are stochastic components. Then, the virtual Rice factor $K^{\mathrm{vir}}(t)$ can be expressed as

$$K^{\mathrm{vir}}(t)=\frac{\Omega_{\mathrm{TR}}^{\mathrm{RIS}_1}(t)}{\Omega_{\mathrm{TR}}^{\mathrm{RIS}_2}(t)+\Omega_{\mathrm{TR}}^{\mathrm{RIS}_{12}}(t)+\Omega_{\mathrm{TR}}^{\mathrm{cluster}}(t)}, \tag{26}$$

and Eq. (6) can be rewritten as follows:

$$\begin{aligned}
&h_{pq}(t,\tau)\\
&=\sqrt{\frac{K^{\mathrm{vir}}(t)}{K^{\mathrm{vir}}(t)+1}}\,h_{pq}^{\mathrm{RIS}_1}(t)\delta\big(\tau-\tau^{\mathrm{RIS}_1}(t)\big)\\
&\quad+\sqrt{\frac{1}{K^{\mathrm{vir}}(t)+1}}\sqrt{\frac{\Omega_{\mathrm{TR}}^{\mathrm{RIS}_2}(t)}{\Omega_{II}}}\,h_{pq}^{\mathrm{RIS}_2}(t)\delta\big(\tau-\tau^{\mathrm{RIS}_2}(t)\big)\\
&\quad+\sqrt{\frac{1}{K^{\mathrm{vir}}(t)+1}}\sqrt{\frac{\Omega_{\mathrm{TR}}^{\mathrm{RIS}_{12}}(t)}{\Omega_{II}}}\,h_{pq}^{\mathrm{RIS}_{12}}(t)\delta\big(\tau-\tau^{\mathrm{RIS}_{12}}(t)\big)\\
&\quad+\sqrt{\frac{1}{K^{\mathrm{vir}}(t)+1}}\sqrt{\frac{\Omega_{\mathrm{TR}}^{\mathrm{cluster}}(t)}{\Omega_{II}}}\,h_{pq}^{\mathrm{cluster}}(t)\delta\big(\tau-\tau^{\mathrm{cluster}}(t)\big),
\end{aligned} \tag{27}$$

where $\Omega_{II}=\Omega_{\mathrm{TR}}^{\mathrm{RIS}_2}(t)+\Omega_{\mathrm{TR}}^{\mathrm{RIS}_{12}}(t)+\Omega_{\mathrm{TR}}^{\mathrm{cluster}}(t)$.

Case III: RIS$_1$ adopts a random reflection phase configuration while RIS$_2$ adopts the optimal phase configuration. In this case, $h_{pq}^{\mathrm{RIS}_2}(t)$ is a deterministic component, while $h_{pq}^{\mathrm{RIS}_1}(t)$ and $h_{pq}^{\mathrm{RIS}_{12}}(t)$ are stochastic components. Then, the virtual Rice factor $K^{\mathrm{vir}}(t)$ can be expressed as

$$K^{\mathrm{vir}}(t)=\frac{\Omega_{\mathrm{TR}}^{\mathrm{RIS}_2}(t)}{\Omega_{\mathrm{TR}}^{\mathrm{RIS}_1}(t)+\Omega_{\mathrm{TR}}^{\mathrm{RIS}_{12}}(t)+\Omega_{\mathrm{TR}}^{\mathrm{cluster}}(t)}, \tag{28}$$

and Eq. (6) can be rewritten as follows:

$$\begin{aligned}
&h_{pq}(t,\tau)\\
&=\sqrt{\frac{K^{\mathrm{vir}}(t)}{K^{\mathrm{vir}}(t)+1}}\,h_{pq}^{\mathrm{RIS}_2}(t)\delta\big(\tau-\tau^{\mathrm{RIS}_2}(t)\big)\\
&\quad+\sqrt{\frac{1}{K^{\mathrm{vir}}(t)+1}}\sqrt{\frac{\Omega_{\mathrm{TR}}^{\mathrm{RIS}_1}(t)}{\Omega_{III}}}\,h_{pq}^{\mathrm{RIS}_1}(t)\delta\big(\tau-\tau^{\mathrm{RIS}_1}(t)\big)\\
&\quad+\sqrt{\frac{1}{K^{\mathrm{vir}}(t)+1}}\sqrt{\frac{\Omega_{\mathrm{TR}}^{\mathrm{RIS}_{12}}(t)}{\Omega_{III}}}\,h_{pq}^{\mathrm{RIS}_{12}}(t)\delta\big(\tau-\tau^{\mathrm{RIS}_{12}}(t)\big)\\
&\quad+\sqrt{\frac{1}{K^{\mathrm{vir}}(t)+1}}\sqrt{\frac{\Omega_{\mathrm{TR}}^{\mathrm{cluster}}(t)}{\Omega_{III}}}\,h_{pq}^{\mathrm{cluster}}(t)\delta\big(\tau-\tau^{\mathrm{cluster}}(t)\big),
\end{aligned} \tag{29}$$

where $\Omega_{III}=\Omega_{\mathrm{TR}}^{\mathrm{RIS}_1}(t)+\Omega_{\mathrm{TR}}^{\mathrm{RIS}_{12}}(t)+\Omega_{\mathrm{TR}}^{\mathrm{cluster}}(t)$.

Case IV: RIS$_1$ and RIS$_2$ both adopt random reflection phase configurations. In this case, $h_{pq}^{\mathrm{RIS}_1}(t)$, $h_{pq}^{\mathrm{RIS}_2}(t)$, and $h_{pq}^{\mathrm{RIS}_{12}}(t)$ in Eq. (6) are all stochastic components, and the Rice factor $K^{\mathrm{vir}}(t)=0$. Specifically, when RIS$_1$ and RIS$_2$ both adopt random uniform phase configurations and meanwhile the numbers of RIS units are large enough, $h_{pq}(t,\tau)$ is characterized by Rayleigh fading under the Central Limit Theorem.

It is worth mentioning that the reflection phase configuration of the propagation link through single-RIS is significantly different from that through double-RIS. Specifically, the optimal reflection phase configuration of the UAV $\rightarrow$ RIS$_{1(2)}$ $\rightarrow$ GR propagation link can be obtained by optimizing the RIS$_{(1(2))}$ phase configurations. This aims at compensating the phase difference between different transmit-receive pairs of single-RIS propagation links to achieve the maximum power gain. However, the optimal reflection phase configuration of the UAV $\rightarrow$ RIS$_1$ $\rightarrow$ RIS$_2$ $\rightarrow$ GR propagation link can be obtained through the joint optimization of RIS$_1$ and RIS$_2$ phase configurations, which aims at compensating the phase difference between different transmit-receive pairs of the double-RIS propagation links to achieve the maximum power gain. Furthermore, when RIS$_1$ and RIS$_2$ both adopt optimal reflection phase configurations, the path gain of the UAV $\rightarrow$ RIS$_1$ $\rightarrow$ RIS$_2$ $\rightarrow$ GR propagation link is not optimal compared to that of the UAV $\rightarrow$ RIS$_1$ $\rightarrow$ GR propagation link or the UAV $\rightarrow$ RIS$_2$ $\rightarrow$ GR propagation link. To sum up, the abovementioned optimal reflection phase configurations have two meanings. The first one is the optimal phase for the propagation links through single-RIS, the other is the jointly optimal phase for the propagation links through double-RIS.

III. Statistical Properties of the Proposed Channel Model

In this section, we first study the fading characteristics of the proposed channel model. Then, we derive and investigate

the channel propagation characteristics, including time-varying spatial-temporal (ST) CCFs, temporal ACFs, and FCFs.

A. Fading Characteristics

In traditional channels without RIS, the attenuation of propagation channel model between the UAV and GR is featured with the Rayleigh fading effect when the direct propagation path is blocked. However, when we consider the double-RIS in UAV-to-ground channels, the fading can be described by the Rician fading with the virtual Rice factor $K^{\text{vir}}(t)$, in which the propagation path(s) through the double-RIS behave similar to the LoS path and supply a definite component on the received signals. Specifically, when the reflection phases at RIS_1 and RIS_2 are both random uniform phases, $\varphi_{m_1,n_1}(t) \sim \text{U}[-\pi,\pi)$ and $\varphi_{m_2,n_2}(t) \sim \text{U}[-\pi,\pi)$; otherwise, $h_{pq}(t,\tau)$ can be characterized by the Rayleigh fading.

B. ST CCFs

In the proposed channel model, the local correlation properties of two arbitrary CIRs, i.e., $h_{pq}(t,\tau)$ and $h_{p'q'}(t,\tau)$, are completely determined by the correlation properties of $h_{pq}(t)$ and $h_{p'q'}(t+\Delta t)$, in which $p' = 1,2,\ldots,M_T$ and $q' = 1,2,\ldots,M_R$. Consequently, there are no correlations between the underlying processes in different propagation delays and in different kinds of propagation paths [26]. Then, we have

$$\rho_{(p,q),(p',q')}(t,\Delta p,\Delta q,\Delta t) = \frac{\mathbb{E}\left[h_{pq}(t)h^*_{p'q'}(t+\Delta t)\right]}{\sqrt{\mathbb{E}\left[|h_{pq}(t)|^2\right]\mathbb{E}\left[|h_{p'q'}(t+\Delta t)|^2\right]}}, \quad (30)$$

where Δt represents the time difference; $\Delta p = |k_{p'} - k_p|\delta_T/\lambda$ and $\Delta q = |k_{q'} - k_q|\delta_R/\lambda$ are the regularized antenna spacings of the UAV and GR antenna arrays, respectively; p, p', q, and q' are the antenna indices. Through the substitution of Eq. (6) into Eq. (30), the ST CCF between the (p,q)-th and the (p',q')-th antenna pairs of the propagation links in the proposed channel model can be written as

$$\begin{aligned}&\rho_{(p,q),(p',q')}(t,\Delta p,\Delta q,\Delta t)\\ &= \rho^{\text{RIS}_1}_{(p,q),(p',q')}(t,\Delta p,\Delta q,\Delta t) + \rho^{\text{RIS}_2}_{(p,q),(p',q')}(t,\Delta p,\Delta q,\Delta t)\\ &\quad + \rho^{\text{RIS}_{12}}_{(p,q),(p',q')}(t,\Delta p,\Delta q,\Delta t) + \rho^{\text{cluster}}_{(p,q),(p',q')}(t,\Delta p,\Delta q,\Delta t),\end{aligned} \quad (31)$$

where $\rho^{\text{RIS}_1}_{(p,q),(p',q')}(t,\Delta p,\Delta q,\Delta t)$ stands for the ST CCF of UAV $\rightarrow$ RIS_1 $\rightarrow$ GR propagation link, and it can be described as By replacing all the $[\cdot]_1$ subscripts in Eq. (32), as shown at the bottom of the next page, with the $[\cdot]_2$ subscript, the ST CCF of RIS_2 propagation link can be acquired. Here, omit them here for brevity. Furthermore, in Eq. (31), $\rho^{\text{RIS}_{12}}_{(p,q),(p',q')}(t,\Delta p,\Delta q,\Delta t)$ is the ST CCF of the UAV $\rightarrow$ RIS_1 $\rightarrow$ RIS_2 $\rightarrow$ GR link, which can be written as With respect to investigation of the channel propagation characteristics for NLoS links, it is crucial to assume that the NLoS propagation links follow the complex Gaussian distribution. To achieve this goal, the number of NLoS rays within the cluster is assumed to tend to infinity, i.e., $L \rightarrow \infty$, which enables the complex CIR $h^{\text{cluster}}_{pq}(t)$ of NLoS propagation links to satisfy the Central Limit Theorem [27]. Thus, the sum of infinite scatterers can be replaced by the integrals of $\alpha_{R,\text{cluster}}$ and $\beta_{R,\text{cluster}}$, respectively. Then, we have

$$\begin{aligned}&\rho^{\text{cluster}}_{(p,q),(p',q')}(t,\Delta p,\Delta q,\Delta t)\\ &= \sqrt{\frac{\Omega^{\text{cluster}}_{\text{TR}}(t)\,\Omega^{\text{cluster}}_{\text{TR}}(t+\Delta t)}{\Omega^{\text{large}}_{\text{TR}}(t)\,\Omega^{\text{large}}_{\text{TR}}(t+\Delta t)}} \times \int_{-\pi}^{\pi}\int_{-\pi}^{\pi}\\ &\quad \times e^{-j\frac{2\pi}{\lambda}\left(\xi_{p,\text{cluster}}(t)-\xi_{p',\text{cluster}}(t+\Delta t)+\xi_{q,\text{cluster}}(t)-\xi_{q',\text{cluster}}(t+\Delta t)\right)}\\ &\quad \times e^{j\frac{2\pi}{\lambda}v_T t\cos\left(\alpha_{T,\text{cluster}}(t)-\eta_T\right)\cos\beta_{T,\text{cluster}}(t)\cos\gamma_T}\\ &\quad \times e^{-j\frac{2\pi}{\lambda}v_T(t+\Delta t)\cos\left(\alpha_{T,\text{cluster}}(t+\Delta t)-\eta_T\right)\cos\beta_{T,\text{cluster}}(t+\Delta t)\cos\gamma_T}\\ &\quad \times e^{j\frac{2\pi}{\lambda}\left[v_T t\sin\beta_{T,\text{cluster}}(t)\sin\gamma_T - v_T(t+\Delta t)\sin\beta_{T,\text{cluster}}(t+\Delta t)\sin\gamma_T\right]}\\ &\quad \times e^{j\frac{2\pi}{\lambda}v_R t\cos\left(\alpha_{R,\text{cluster}}(t)-\eta_R\right)\cos\beta_{R,\text{cluster}}(t)}\\ &\quad \times e^{-j\frac{2\pi}{\lambda}v_R(t+\Delta t)\cos\left(\alpha_{R,\text{cluster}}(t+\Delta t)-\eta_R\right)\cos\beta_{R,\text{cluster}}(t+\Delta t)}\\ &\quad \times f(\alpha_{R,\text{cluster}},\beta_{R,\text{cluster}})d(\alpha_{R,\text{cluster}},\beta_{R,\text{cluster}})\ .\end{aligned} \quad (34)$$

where $f(\alpha_{R,\text{cluster}},\beta_{R,\text{cluster}})$ represents the joint probability density function (PDF) of the received azimuth $\alpha_{R,\text{cluster}}$ and elevation $\beta_{R,\text{cluster}}$ angles. Since the ray directions of each cluster are commonly confined in these propagations, we can use the truncated Gaussian distribution to characterize the UAV-to-ground channel model [23]. The wave in the ϑ direction, which is confined to the PDF between ϑ_{up} and ϑ_{low}, can be represented as

$$f\left(\vartheta,\mu_\vartheta,\sigma_\vartheta,\vartheta_{\text{low}},\vartheta_{\text{up}}\right) = \frac{\frac{1}{\sigma_\vartheta}u\left(\frac{\vartheta-\mu_\vartheta}{\sigma_\vartheta}\right)}{\Phi\left(\frac{\vartheta_{\text{up}}-\mu_\vartheta}{\sigma_\vartheta}\right)-\Phi\left(\frac{\vartheta_{\text{low}}-\mu_\vartheta}{\sigma_\vartheta}\right)}, \quad (35)$$

where μ_ϑ and $\sigma_\vartheta = \vartheta_{\text{up}} - \vartheta_{\text{low}}$ are the angular distribution and the mean value of the signal direction $\vartheta \in [\,\vartheta_{\text{low}},\vartheta_{\text{up}}\,]$, respectively; $u(\kappa)$ is the PDF of a stochastic variable κ following the standard normal distribution, which can be expressed as $u(\kappa) = \frac{1}{\sqrt{2\pi}}\exp\{-\frac{\kappa^2}{2}\}$; $\Phi(\kappa) = \int_{-\infty}^{\kappa}u(\kappa')d\kappa' = \frac{1}{2}\left(1+\text{erf}(\frac{\kappa}{\sqrt{2}})\right)$ represents the cumulative distribution function of a stochastic variable κ following the standard normal distribution, in which $\text{erf}(\cdot)$ is applied as a Gauss error function. Since the elevation and azimuth signal angles are typically considered to be mutually independent, the joint PDF $f(\alpha_{R,\text{cluster}},\beta_{R,\text{cluster}})$ in Eq. (34) can be further written as

$$\begin{aligned}&f(\alpha_{R,\text{cluster}},\beta_{R,\text{cluster}})\\ &= f\left(\alpha_{R,\text{cluster}},\mu_{\alpha_{R,\text{cluster}}},\sigma_{\alpha_{R,\text{cluster}}},\alpha^{\text{low}}_{R,\text{cluster}},\alpha^{\text{up}}_{R,\text{cluster}}\right)\\ &\quad \times f\left(\beta_{R,\text{cluster}},\mu_{\beta_{R,\text{cluster}}},\sigma_{\beta_{R,\text{cluster}}},\beta^{\text{low}}_{R,\text{cluster}},\beta^{\text{up}}_{R,\text{cluster}}\right).\end{aligned} \quad (36)$$

It is worthy to note that the time-varying propagation distances and angles in Eqs. (32)-(34) are associated with the motion velocity/direction/time of the UAV and GR, which implies that the motion properties of the transceivers have certain influences on the ST CCFs of two different propagation links in the proposed channel model. In addition, when we impose $p = p'$ and $q = q'$, i.e., $\Delta p = \Delta q = 0$, Eqs. (32)-(34) can be deduced to the temporal ACFs of the proposed channel model, which have the ability of characterizing the correlation properties of the propagation links in time domain [28].

C. FCFs

Through the relationship between the propagation delay τ and the Fourier transform of $h_{pq}(t,\tau)$ in Eq. (6), the time-invariant transfer function of the proposed channel model can be written as

$$\begin{aligned} H_{pq}(t,f) = &\sqrt{\frac{\Omega_{\mathrm{TR}}^{\mathrm{RIS}_1}(t)}{\Omega_{\mathrm{TR}}^{\mathrm{large}}(t)}} h_{pq}^{\mathrm{RIS}_1}(t) e^{-j2\pi f \tau^{\mathrm{RIS}_1}(t)} \\ &+ \sqrt{\frac{\Omega_{\mathrm{TR}}^{\mathrm{RIS}_2}(t)}{\Omega_{\mathrm{TR}}^{\mathrm{large}}(t)}} h_{pq}^{\mathrm{RIS}_2}(t) e^{-j2\pi f \tau^{\mathrm{RIS}_2}(t)} \\ &+ \sqrt{\frac{\Omega_{\mathrm{TR}}^{\mathrm{RIS}_{12}}(t)}{\Omega_{\mathrm{TR}}^{\mathrm{large}}(t)}} h_{pq}^{\mathrm{RIS}_{12}}(t) e^{-j2\pi f \tau^{\mathrm{RIS}_{12}}(t)} \\ &+ \sqrt{\frac{\Omega_{\mathrm{TR}}^{\mathrm{cluster}}(t)}{\Omega_{\mathrm{TR}}^{\mathrm{large}}(t)}} h_{pq}^{\mathrm{cluster}}(t) e^{-j2\pi f \tau^{\mathrm{cluster}}(t)}, \end{aligned} \tag{37}$$

Then, the FCF for the (p,q)-th antenna pair of the propagation link model can be represented as

$$\rho_{H_{pq}}(t,\Delta f) = \frac{\mathbb{E}\big[H_{pq}(t) H_{pq}^*(f+\Delta f)\big]}{\sqrt{\mathbb{E}\big[|H_{pq}(t)|^2\big]\mathbb{E}\big[|H_{pq}(f+\Delta f)|^2\big]}}, \tag{38}$$

where Δf represents the frequency separation. By substituting Eq. (37) into Eq. (38), the FCF of the proposed channel model can be written as

$$\begin{aligned} &\rho_{H_{pq}}(t,\Delta f) \\ &= \frac{\Omega_{\mathrm{TR}}^{\mathrm{cluster}}(t)}{\Omega_{\mathrm{TR}}^{\mathrm{large}}(t)} \sum_{\ell=1}^{L} e^{-j2\pi\Delta f \tau^{\mathrm{cluster}}(t)} + \frac{\Omega_{\mathrm{TR}}^{\mathrm{RIS}_1}(t)}{\Omega_{\mathrm{TR}}^{\mathrm{large}}(t)} e^{-j2\pi\Delta f \tau^{\mathrm{RIS}_1}(t)} \\ &\quad + \frac{\Omega_{\mathrm{TR}}^{\mathrm{RIS}_2}(t)}{\Omega_{\mathrm{TR}}^{\mathrm{large}}(t)} e^{-j2\pi\Delta f \tau^{\mathrm{RIS}_2}(t)} + \frac{\Omega_{\mathrm{TR}}^{\mathrm{RIS}_{12}}(t)}{\Omega_{\mathrm{TR}}^{\mathrm{large}}(t)} e^{-j2\pi\Delta f \tau^{\mathrm{RIS}_{12}}(t)}. \end{aligned} \tag{39}$$

As can be seen, the FCF of the proposed channel model is correlated with the frequency separation Δf and the motion time t, but not with the frequency f. This implies that the channel model is non-stationary in time domain, but stationary in frequency domain. In addition, this also means that the reflection phase configurations of double-RIS play an important role in the FCF, which is a specific feature of double-RIS cooperatively assisted UAV-to-ground channels.

IV. Numerical Results and Discussions

In this section, we examine the propagation properties of the proposed channel model through comparing the computer simulation results and theoretical results.

A. Parameter Settings of Numerical Simulation

In our numerical simulation, the parameter settings, which are basically consistent with the settings of channel measurement, are given as follows unless specified otherwise: $f_c = 5$ GHz, $M_T = 4$, $M_R = 6$, $\delta_T = \delta_R = \lambda/2$, $\psi_T = \pi/3$, $\phi_T = \pi/4$, $\psi_R = \pi/4$, $\phi_R = \pi/4$, $H_0 = 50$ m, and $D_0 = 100$ m; for NLoS links via the cluster, $\alpha_{R,\mathrm{cluster}} = 2\pi/3$,

$$\begin{aligned} &\rho_{(p,q),(p',q')}^{\mathrm{RIS}_1}(t,\Delta p,\Delta q,\Delta t) \\ &= \sqrt{\frac{\Omega_{\mathrm{TR}}^{\mathrm{RIS}_1}(t)\,\Omega_{\mathrm{TR}}^{\mathrm{RIS}_1}(t+\Delta t)}{\Omega_{\mathrm{TR}}^{\mathrm{large}}(t)\,\Omega_{\mathrm{TR}}^{\mathrm{large}}(t+\Delta t)}} \frac{1}{\sqrt{\Upsilon_{pq}^{\mathrm{RIS}_1}(t)\Upsilon_{p'q'}^{\mathrm{RIS}_1}(t+\Delta t)}} \times \mathbb{E}\Big\{ \sum_{m_1=1}^{M_1}\sum_{n_1=1}^{N_1}\sum_{m_1'=1}^{M_1}\sum_{n_1'=1}^{N_1} \chi_{m_1,n_1}(t)\ \chi_{m_1',n_1'}(t+\Delta t) \\ &\times e^{j\left(\varphi_{m_1,n_1}(t)-\varphi_{m_1',n_1'}(t+\Delta t)\right)} e^{-j\frac{2\pi}{\lambda}\left(\xi_{p,(m_1,n_1)}(t)-\xi_{p',(m_1',n_1')}(t+\Delta t)+\xi_{q,(m_1,n_1)}(t)-\xi_{q',(m_1',n_1')}(t+\Delta t)\right)} \\ &\times e^{j\frac{2\pi}{\lambda}\left[v_R t\cos\left(\alpha_{R,(m_1,n_1)}(t)-\eta_R\right)\cos\beta_{R,(m_1,n_1)}(t)-v_R(t+\Delta t)\cos\left(\alpha_{R,(m_1',n_1')}(t+\Delta t)-\eta_R\right)\cos\beta_{R,(m_1',n_1')}(t+\Delta t)\right]} \\ &\times e^{j\frac{2\pi}{\lambda}v_T t\left(\cos\left(\alpha_{T,(m_1,n_1)}(t)-\eta_T\right)\cos\beta_{T,(m_1,n_1)}(t)\cos\gamma_T+\sin\beta_{T,(m_1,n_1)}(t)\sin\gamma_T\right)} \\ &\times e^{-j\frac{2\pi}{\lambda}v_T(t+\Delta t)\left(\cos\left(\alpha_{T,(m_1',n_1')}(t+\Delta t)-\eta_T\right)\cos\beta_{T,(m_1',n_1')}(t+\Delta t)\cos\gamma_T+\sin\beta_{T,(m_1',n_1')}(t+\Delta t)\sin\gamma_T\right)} \Big\}, \end{aligned} \tag{32}$$

$$\begin{aligned} &\rho_{(p,q),(p',q')}^{\mathrm{RIS}_{12}}(t,\Delta p,\Delta q,\Delta t) \\ &= \sqrt{\frac{\Omega_{\mathrm{TR}}^{\mathrm{RIS}_{12}}(t)\Omega_{\mathrm{TR}}^{\mathrm{RIS}_{12}}(t+\Delta t)}{\Omega_{\mathrm{TR}}^{\mathrm{large}}(t)\Omega_{\mathrm{TR}}^{\mathrm{large}}(t+\Delta t)}} \times \frac{1}{\sqrt{\Upsilon_{pq}^{\mathrm{RIS}_{12}}(t)\Upsilon_{p'q'}^{\mathrm{RIS}_{12}}(t+\Delta t)}} \\ &\times \mathbb{E}\Big\{ \sum_{m_2=1}^{M_2}\sum_{n_2=1}^{N_2}\sum_{m_1=1}^{M_1}\sum_{n_1=1}^{N_1}\sum_{m_2'=1}^{M_2}\sum_{n_2'=1}^{N_2}\sum_{m_1'=1}^{M_1}\sum_{n_1'=1}^{N_1} \chi_{m_1,n_1}(t)\ \chi_{m_2,n_2}(t) \\ &\times \chi_{m_1',n_1'}(t+\Delta t)\chi_{m_2',n_2'}(t+\Delta t) e^{j\left(\varphi_{m_1,n_1}(t)+\varphi_{m_2,n_2}(t)\right)} e^{-j\left(\varphi_{m_1',n_1'}(t+\Delta t)+\varphi_{m_2',n_2'}(t+\Delta t)\right)} \\ &\times e^{-j\frac{2\pi}{\lambda}\left(\xi_{p,(m_1,n_1)}(t)-\xi_{p',(m_1',n_1')}(t+\Delta t)+\xi_{q,(m_2,n_2)}(t)-\xi_{q',(m_2',n_2')}(t+\Delta t)\right)} \\ &\times e^{j\frac{2\pi}{\lambda}v_T t\left(\cos\left(\alpha_{T,(m_1,n_1)}(t)-\eta_T\right)\cos\beta_{T,(m_1,n_1)}(t)\cos\gamma_T+\sin\beta_{T,(m_1,n_1)}(t)\sin\gamma_T\right)} \\ &\times e^{-j\frac{2\pi}{\lambda}v_T(t+\Delta t)\left(\cos\left(\alpha_{T,(m_1',n_1')}(t+\Delta t)-\eta_T\right)\cos\beta_{T,(m_1',n_1')}(t+\Delta t)\cos\gamma_T+\sin\beta_{T,(m_1',n_1')}(t+\Delta t)\sin\gamma_T\right)} \\ &\times e^{j\frac{2\pi}{\lambda}\left[v_R t\cos\left(\alpha_{R,(m_2,n_2)}(t)-\eta_R\right)\cos\beta_{R,(m_2,n_2)}(t)-v_R(t+\Delta t)\cos\left(\alpha_{R,(m_2',n_2')}(t+\Delta t)-\eta_R\right)\cos\beta_{R,(m_2',n_2')}(t+\Delta t)\right]} \Big\}, \end{aligned} \tag{33}$$

$\mu_{\alpha_{R,\text{cluster}}} = \pi/6$, $\beta_{R,\text{cluster}} = \pi/4$, and $\mu_{\beta_{R,\text{cluster}}} = \pi/12$; for RIS propagation links, $\chi_{m_1,n_1}(t) = 1$, $M_1 = N_1 = 100$, $d_{M_1} = d_{N_1} = \lambda/4$, $x_{\text{RIS}_1} = 20$ m, $y_{\text{RIS}_1} = 20$ m, $z_{\text{RIS}_1} = 25$ m, and $\theta_{\text{RIS}_1} = -\pi/18$ for RIS_1, whereas $\chi_{m_2,n_2}(t) = 1$, $M_2 = N_2 = 100$, $d_{M_2} = d_{N_2} = \lambda/4$, $x_{\text{RIS}_2} = 80$ m, $y_{\text{RIS}_2} = -20$ m, $z_{\text{RIS}_2} = 25$ m, and $\theta_{\text{RIS}_2} = \pi/18$ for RIS_2; for UAV, $v_T = 5$ m/s, $\eta_T = 0$, and $\gamma_T = 0$; for GR, $v_R = 2$ m/s and $\eta_R = \pi$.

B. Performance Analysis

1) Fading Characterization: Fig. 2 shows the fading characteristics of the proposed channel model for different reflection phase configurations of the RISs. Figs. 2(a), 2(b), and 2(c) correspond to the reflection phase configurations for Case I, Case II, and Case II, respectively. As can be observed, the channel model tends to be characterized by the Rician fading as RIS_1 and/or RIS_2 adopt(s) the optimal phase configurations. Fig. 2(d) corresponds to the reflection phase configurations for Case IV. When RIS_1 and RIS_2 both adopt random phase configurations, the proposed channel model can be roughly characterized by the Rayleigh fading. Based on the aforementioned observations, it can be concluded that the proposed channel model displays different fading characteristics under different settings of RIS phase configurations. This implies that the physical properties of RISs have significant influences on the double-RIS assisted UAV-to-ground channel propagation characteristics.

2) Path Power Gains: Under the RIS reflection phase configurations for Case I, Fig. 3 displays the path power gains of $\text{RIS}_{1(2)}$ propagation links of the proposed channel model for different RIS orientation angles. As can be seen, the path power gain exhibits different values at different motion time t, indicating the channel non-stationarity in time domain. Furthermore, it is noticed that the path power gain of the wave experiencing $\text{RIS}_{1(2)}$ propagation links is superior to that of the wave experiencing LoS links, confirming the extensible capacity by introducing RIS into UAV communication systems. In addition, it can be concluded that the rotation angles θ_{RIS_1} and θ_{RIS_2} have significant influences on the path power gains of RIS_1 and RIS_2 propagation links, respectively. This implies that the investigation on the fading characteristics of the proposed channel model needs to consider different RISs configurations and orientations.

Fig. 4 shows the path power gains of the propagation links through single- and double-RIS for different RIS orientation angles under the RIS reflection phase configurations for Case I. When RIS_1 and RIS_2 independently optimize the phase configurations, the power transmitted from RIS_1 to RIS_2 is extremely small, which cause a very small path power gain for the UAV $\rightarrow$ RIS_1 $\rightarrow$ RIS_2 $\rightarrow$ GR link. However, when RIS_1 and RIS_2 jointly optimize the phase configurations, the path power gain of the double-RIS propagation link decays with the decrease of θ_{RIS_2} from $\pi/18$ to $-\pi/18$. In this case, the path power gain generally increases to a peak value first and then gradually decreases with increasing motion time, and its changing trend is basically in agreement with the results in Fig. 3. On the whole, the path power gain of the propagation links through double-RIS is larger than that of the propagation links through single-RIS or LoS link, thereby demonstrating the desirable performance of introducing double-RIS into wireless channels.

3) Spatial CCFs: Fig. 5 presents the spatial CCFs of the proposed channel model for different UAV heights under the RIS reflection phase configurations for Case III. Since Eq. (31) involves a Bessel function, the correlation properties in spatial domain decrease with fluctuation as the antenna spacing at the GR increases. These are consistent with the computer simulation results in [26] and [28] and the measurement results in [29], thereby validating the accuracy of the derived spatial CCFs of the proposed channel model. It is worth mentioning that the spatial CCFs of the propagation links through single- and double-RIS, i.e., $\rho^{\text{RIS}_1}_{(p,q),(p',q')}(t,\Delta p,\Delta q)$, $\rho^{\text{RIS}_2}_{(p,q),(p',q')}(t,\Delta p,\Delta q)$, and $\rho^{\text{RIS}_{12}}_{(p,q),(p',q')}(t,\Delta p,\Delta q)$, are complex exponential functions of the antenna spacing with constant absolute value; however, the spatial CCF of the NLoS link, i.e., $\rho^{\text{cluster}}_{(p,q),(p',q')}(t,\Delta p,\Delta q)$, is a complex exponential function of antenna spacing with reduced absolute value. Hence, the linearly superimposed curves of the spatial CCFs of the propagation links in the proposed channel model also follow a complex exponential function of antenna spacing. Furthermore, it is noticed that different UAV altitudes can lead to different spatial correlations, demonstrating the spatial non-stationarity of the proposed channel model [20].

Fig. 6 presents the spatial CCFs of the propagation links for different RISs reflection phase configurations at $t = 2$. As RIS_1 or/and RIS_2 adopt(s) the optimal phase configuration(s), the decline of the spatial CCFs, which is similar to that of the LoS links, can be observed. This means that the UAV $\rightarrow$ RIS_1 $\rightarrow$ GR link, UAV $\rightarrow$ RIS_2 $\rightarrow$ GR link, and UAV $\rightarrow$ RIS_1 $\rightarrow$ RIS_2 $\rightarrow$ GR link perform similar propagation properties to those of the physical LoS link. Furthermore, when RIS_1 and RIS_2 both adopt random phase configurations, the spatial correlation of the double-RIS propagation link is consistent with that of the NLoS link because of the extremely small power gains. On the whole, the phase configurations of RISs have significant influences on the spatial correlations of the propagation links. This can be an important issue for the design and evaluation of the double-RIS assisted UAV-to-ground communication systems.

4) Temporal ACFs: Fig. 7 shows the temporal ACFs of the proposed channel model for different RIS reflection phase configurations. It can be seen that the temporal correlations progressively attenuate as the time difference Δt increases, demonstrating the channel non-stationarity in time domain. These results are in accordance with the computer simulation results in [30], thus verifying the accuracy of the derivation of the temporal ACFs of the proposed channel model. Furthermore, the temporal ACFs generally change more slightly with less fluctuations compared to the changing trends of the spatial CCFs in Figs. 5 and 6. Moreover, it is noticed that different optimization characteristics of RIS can result in different temporal correlations of the proposed channel model, which agrees very well with the observation results of the spatial CCFs in Fig. 6.

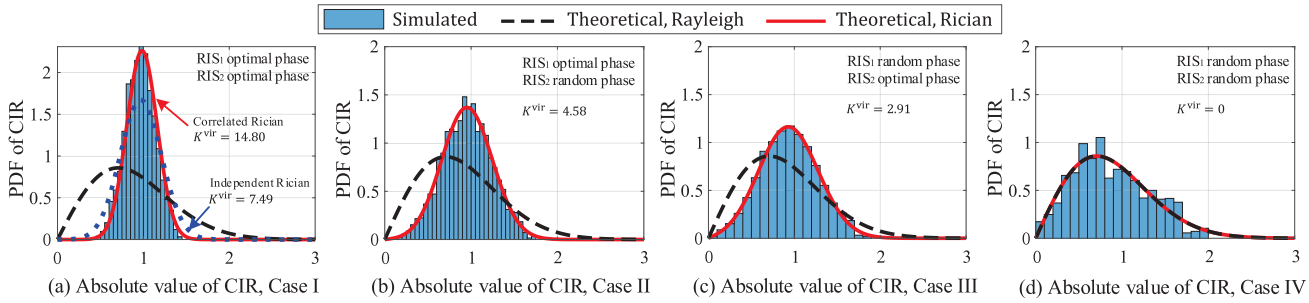

Fig. 2. Fading characteristics of the proposed channel model under different RIS reflection phase configurations at $t = 0$ s.

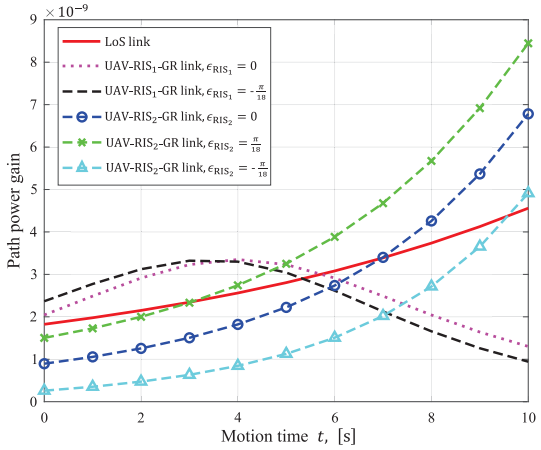

Fig. 3. Path power gains of the $\text{RIS}_{1(2)}$ propagation link under different RIS orientation angles.

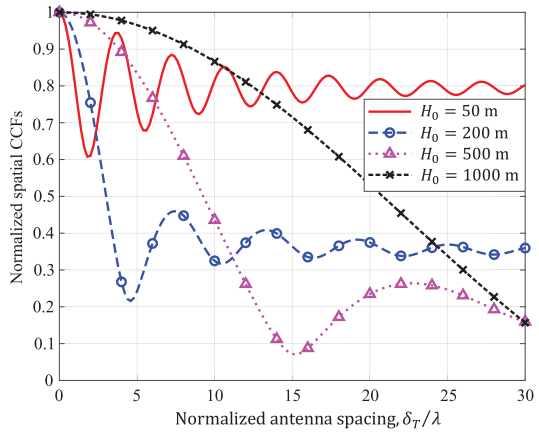

Fig. 5. Spatial CCFs of the proposed channel model under different UAV heights H_0 when $t = 2$ s.

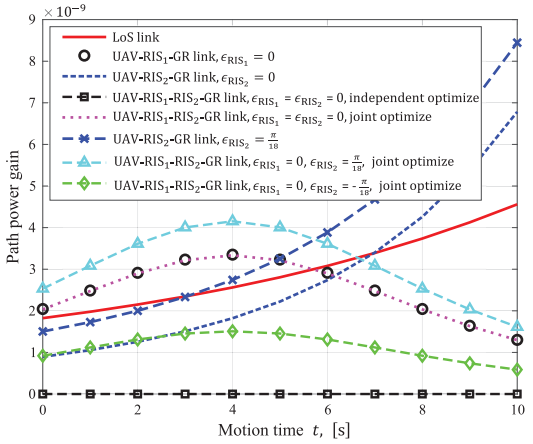

Fig. 4. Path power gains of the propagation links through single- and double-RIS for different RISs orientation angles.

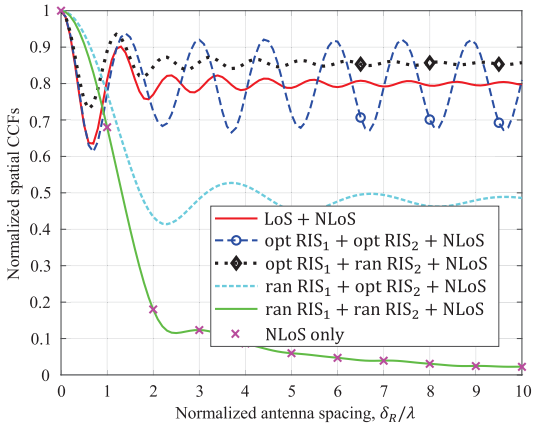

Fig. 6. Spatial CCFs of the proposed channel model under different RIS reflection phase configurations at $t = 2$ s (here, "opt" means "optimal RIS reflection phase configuration" and "ran" means "random RIS reflection phase configuration").

Previous studies have revealed that UAV motion properties, including the velocity, trajectory, and time, play an important role in the investigation on the UAV-to-ground channel propagation characteristics [20]. Based on the RIS reflection phase configurations for Case IV, Fig. 8 shows the temporal ACFs of the proposed channel model with respect to the motion directions and velocities of the UAV. It can be found that different UAV motion directions lead to different correlations in time domain. Nevertheless, when the UAV moves far away from the GR along the line parallel to the x-axis, i.e., $\gamma_T = 0$ and $\eta_T = \pi$, the temporal correlation is obviously stronger than that when the UAV moves towards the GR along the line paralleling to the x-axis, i.e., $\gamma_T = 0$ and $\eta_T = 0$. Moreover, the proposed temporal correlations vary more significantly as the UAV velocity increases from 5 to 10 m/s [20]. Hence, for the purpose of improving the communication quality, the UAV should move away from the GR to achieve high temporal correlations.

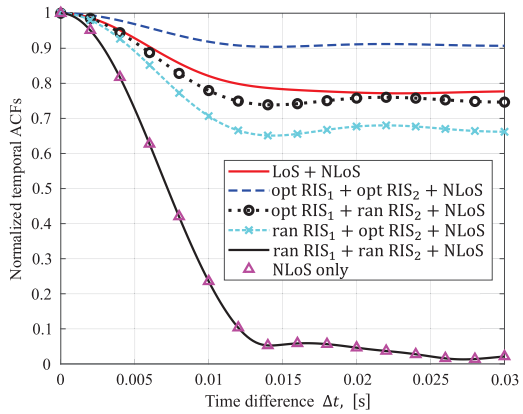

Fig. 7. Temporal ACFs of the proposed channel model under different RISs reflection phase configurations at $t = 5$ s (here, "opt" means "optimal RIS reflection phase configuration" and "ran" means "random RIS reflection phase configuration"; $v_T = 5$ m/s, $\gamma_T = -\pi/6$, $\eta_T = \pi/24$, $v_R = 2$ m/s, and $\eta_R = \pi/6$).

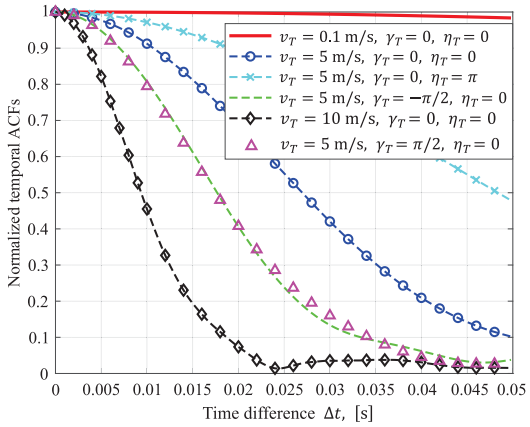

Fig. 8. Temporal ACFs of the proposed channel model under different UAV motion properties when $t = 2$ s, $\theta_{\text{RIS}_1} = \theta_{\text{RIS}_2} = 0$, $v_R = 0.1$ m/s, and $\eta_R = 0$.

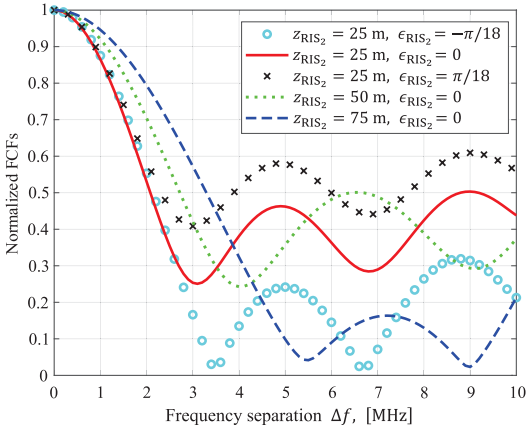

Fig. 9. FCFs of the proposed channel model under different RIS$_2$ positions and orientation angles when $t = 2$ s and $\theta_{\text{RIS}_1} = 0$.

5) Time-Varying FCFs: Based on Eq. (39), Fig. 9 shows the FCFs of the proposed channel model with respect to different positions and horizontal rotation angles of RIS$_2$ under the RIS reflection phase configurations for Case III. As can be seen, there is remarkable difference in the frequency

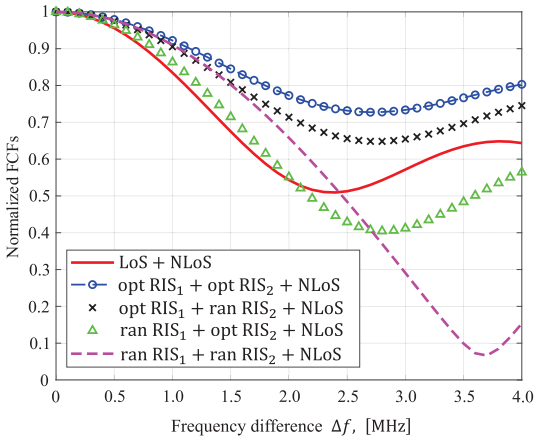

Fig. 10. FCFs of the proposed channel model under different RISs reflection phase configurations at $t = 1$ s (here, "opt" means "optimal RIS reflection phase configuration" and "ran" means "random RIS reflection phase configuration"; $\theta_{\text{RIS}_1} = \theta_{\text{RIS}_2} = 0$).

correlations between two different settings of the positions of RIS$_2$. Furthermore, when the position of RIS$_2$ is fixed, the frequency correlations are enhanced with the increase of θ_{RIS_2} from $-\pi/18$ to $\pi/18$.

Fig. 10 presents the FCFs of the proposed channel model with respect to the different reflection phase configurations of RISs. It can be found that a larger frequency interval Δf leads to a lower value of the frequency correlation, demonstrating the channel non-stationarity in frequency domain. These results align well with those in [31], which confirms the accuracy of the derivation of the FCFs of the proposed channel model. Furthermore, the FCFs show different parameters when we set different phase configurations of RISs. This indicates that the frequency correlations of the proposed channel model are associated with the physical characteristics of the RISs. Specifically, when RIS$_1$ and RIS$_2$ both adopt optimal phase configurations, the frequency correlation is stronger than that in the other cases. However, when RIS$_1$ and RIS$_2$ both adopt random phase configurations, the frequency correlation is obviously lower than that in the other cases.

V. Conclusion

In this paper, we have proposed a 3D physics-based end-to-end channel model for double-RIS cooperatively assisted UAV-to-ground communication channels. By interpreting the complex CIR of the proposed channel model into four distinguishable links, we derive the *path power gains* of different links, enabling the proposed channel model to characterize both large-scale path loss and small-scale fading characteristics in double-RIS assisted UAV-to-ground communication systems. Numerical simulation results have demonstrated that the propagation properties of the proposed channel model, such as spatial CCFs, temporal ACFs, and frequency CFs, are significantly influenced by the reflection phase configurations of the RISs. Moreover, according to the simulation results, the channel characteristics for the double-RIS propagation link behave better than those for the single-RIS link or LoS link, thereby validating the necessity of introducing double-RIS into UAV-to-ground communication.

In our future work, we can state three prospective directions: i) conducting measurements on double-RIS assisted UAV-to-ground communication to further validate the proposed channel modeling solution; ii) developing an effective algorithm to achieve the balance between modeling accuracy and generality; iii) developing an effective algorithm to achieve the balance between communication quality improvement and system complexity.

APPENDIX

For the UAV $\rightarrow$ RIS_1 $\rightarrow$ RIS_2 $\rightarrow$ GR propagation link, when the waves emitted from the UAV impinges on RIS_1, the received power of the (m_1, n_1)-th unit in RIS_1 can be described as

$$P^{\text{in}\rightarrow\text{RIS}_1}_{m_1,n_1}(t) = \frac{P_t G_t \times d_{M_1} d_{N_1} \cos\beta^{\text{in}}_{m_1,n_1}(t)}{4\pi\left(\xi_{T,(m_1,n_1)}(t)\right)^2}, \quad (40)$$

where P_t represents the transmit power; G_t is the UAV transmit antenna gain; $\beta^{\text{in}}_{m_1,n_1}(t)$ is the normal incident angle from the center of the UAV antenna array to the (m_1, n_1)-th unit in RIS_1, which can be derived by

$$\beta^{\text{in}}_{m_1,n_1}(t) = \arccos\left\{\frac{(d_{T,x}(t) - x_{m_1,n_1})\sin\theta_{\text{RIS}_1}}{\|\mathbf{d}_T(t) - \mathbf{d}_{m_1,n_1}\|} - \frac{(d_{T,y}(t) - y_{m_1,n_1})\cos\theta_{\text{RIS}_1}}{\|\mathbf{d}_T(t) - \mathbf{d}_{m_1,n_1}\|}\right\}. \quad (41)$$

In RIS_1, the reflected power of the (m_1, n_1)-th unit can be represented as [32]

$$P^{\text{RIS}_1\rightarrow\text{out}}_{m_1,n_1}(t) = \frac{P_t G_t d_{M_1} d_{N_1}}{4\pi\left(\xi_{T,(m_1,n_1)}(t)\right)^2}\cos\beta^{\text{in}}_{m_1,n_1}(t) \times\left|\chi_{m_1,n_1}(t)e^{j\varphi_{m_1,n_1}(t)}\right|^2. \quad (42)$$

Thus, when the wave manipulated by RIS_1 impinges on RIS_2, the received power of the (m_2, n_2)-th unit in RIS_2 from the (m_1, n_1)-th unit in RIS_1 can be expressed as

$$P^{\text{RIS}_1\rightarrow\text{RIS}_2}_{(m_1,n_1),(m_2,n_2)}(t) = \frac{P_t G_t d_{M_1} d_{N_1}\cos\beta^{\text{in}}_{m_1,n_1}(t)}{4\pi\left(\xi_{T,(m_1,n_1)}(t)\right)^2} \times\left|\chi_{m_1,n_1}(t)e^{j\varphi_{m_1,n_1}(t)}\right|^2 \times\frac{1}{4\pi\left(\xi^{(m_1,n_1)}_{(m_2,n_2)}\right)^2} d_{M_2} d_{N_2}\cos\beta^{\text{in}}_{(m_1,n_1),(m_2,n_2)}, \quad (43)$$

where $\beta^{\text{in}}_{(m_1,n_1),(m_2,n_2)}$ represents the normal incident angle from the (m_1, n_1)-th unit in RIS_1 to the (m_2, n_2)-th unit in RIS_2, which can be derived by

$$\beta^{\text{in}}_{(m_1,n_1),(m_2,n_2)} = \arccos\left\{\frac{(x_{m_1,n_1} - x_{m_2,n_2})\sin\theta_{\text{RIS}_2}}{\|\mathbf{d}_{m_1,n_1} - \mathbf{d}_{m_2,n_2}\|} - \frac{(y_{m_1,n_1} - y_{m_2,n_2})\cos\theta_{\text{RIS}_2}}{\|\mathbf{d}_{m_1,n_1} - \mathbf{d}_{m_2,n_2}\|}\right\}. \quad (44)$$

In RIS_2, the reflected power of the (m_2, n_2)-th unit can be expressed as

$$P^{\text{RIS}_2\rightarrow\text{out}}_{(m_1,n_1),(m_2,n_2)}(t) = \frac{P_t G_t d_{M_1} d_{N_1} d_{M_2} d_{N_2}\cos\beta^{\text{in}}_{m_1,n_1}(t)\ \cos\beta^{\text{in}}_{(m_1,n_1),(m_2,n_2)}}{(4\pi)^2\left(\xi_{T,(m_1,n_1)}(t)\xi^{(m_1,n_1)}_{(m_2,n_2)}\right)^2} \times\left|\chi_{m_1,n_1}(t)\chi_{m_2,n_2}(t)e^{j\varphi_{m_1,n_1}(t)}e^{j\varphi_{m_2,n_2}(t)}\right|^2. \quad (45)$$

The effective aperture of the GR antenna array can be represented as $S_{r,ap} = G_r\lambda^2/4\pi$, in which G_r represents the received antenna gain; the received power from the (m_2, n_2)-th unit in RIS_2 can be computed as

$$P^{\text{RIS}_2\rightarrow\text{GR}}_{(m_1,n_1),(m_2,n_2)}(t) = \frac{P^{\text{RIS}_2\rightarrow\text{out}}_{(m_1,n_1),(m_2,n_2)}(t)}{4\pi\left(\xi_{R,(m_2,n_2)}(t)\right)^2} S_{r,ap}. \quad (46)$$

By substituting Eq. (45) into Eq. (46), we can obtain

$$P^{\text{RIS}_2\rightarrow\text{GR}}_{(m_1,n_1),(m_2,n_2)}(t) = \frac{g_3\cos\beta^{\text{in}}_{m_1,n_1}(t)\ \cos\beta^{\text{in}}_{(m_1,n_1),(m_2,n_2)}}{(4\pi)^4\left(\xi_{T,(m_1,n_1)}(t)\xi^{(m_1,n_1)}_{(m_2,n_2)}\xi_{R,(m_2,n_2)}(t)\right)^2} \times\left|\chi_{m_1,n_1}(t)\chi_{m_2,n_2}(t)e^{j\varphi_{m_1,n_1}(t)}e^{j\varphi_{m_2,n_2}(t)}\right|^2, \quad (47)$$

where $g_3 = P_t G_t G_r \lambda^2 d_{M_1} d_{N_1} d_{M_2} d_{N_2}$. As indicated in [33], the received power $P^{\text{RIS}_2\rightarrow\text{GR}}_{(m_1,n_1),(m_2,n_2)}(t)$ can also be expressed as

$$P^{\text{RIS}_2\rightarrow\text{GR}}_{(m_1,n_1),(m_2,n_2)}(t) = \frac{|E^{\text{RIS}_{12}}_{(m_1,n_1),(m_2,n_2)}(t)|^2}{2\varsigma} S_{r,ap}, \quad (48)$$

where ς and $E^{\text{RIS}_{12}}_{(m_1,n_1),(m_2,n_2)}(t)$ represent the intrinsic impedance ($\simeq 120\pi$ ohms of free-space) and received radiated electric field, respectively. By combination of Eqs. (47) and (48) and considering the phase shift caused by the motion of the UAV and GR, we can derive $E^{\text{RIS}_{12}}_{(m_1,n_1),(m_2,n_2)}(t)$ as below:

$$\begin{aligned} E^{\text{RIS}_{12}}_{(m_1,n_1),(m_2,n_2)}(t) &= \sqrt{\frac{2\varsigma g_3\cos\beta^{\text{in}}_{m_1,n_1}(t)\ \cos\beta^{\text{in}}_{(m_1,n_1),(m_2,n_2)}}{(4\pi)^4 S_{r,ap}}} \\ &\times\frac{\chi_{m_1,n_1}(t)\chi_{m_2,n_2}(t)e^{j\varphi_{m_1,n_1}(t)}e^{j\varphi_{m_2,n_2}(t)}}{\xi_{T,(m_1,n_1)}(t)\xi^{(m_1,n_1)}_{(m_2,n_2)}\xi_{R,(m_2,n_2)}(t)} \\ &\times e^{-j\frac{2\pi}{\lambda}\left(\xi_{T,(m_1,n_1)}(t)+\xi^{(m_1,n_1)}_{(m_2,n_2)}+\xi_{R,(m_1,n_1)}(t)\right)} \\ &\times e^{j\frac{2\pi}{\lambda}v_T t\cos\left(\alpha_{T,(m_1,n_1)}(t)-\eta_T\right)\cos\beta_{T,(m_1,n_1)}(t)\cos\gamma_T} \\ &\times e^{j\frac{2\pi}{\lambda}v_T t\sin\beta_{T,(m_1,n_1)}(t)\sin\gamma_T} \\ &\times e^{j\frac{2\pi}{\lambda}v_R t\cos\left(\alpha_{R,(m_2,n_2)}(t)-\eta_R\right)\cos\beta_{R,(m_2,n_2)}(t)}. \end{aligned} \quad (49)$$

The superposed received electric field can be computed by

$$E_{\text{RIS}_{12}}(t) = \sum_{m_2=1}^{M_2}\sum_{n_2=1}^{N_2}\sum_{m_1=1}^{M_1}\sum_{n_1=1}^{N_1} E^{\text{RIS}_{12}}_{(m_1,n_1),(m_2,n_2)}(t). \quad (50)$$

At the receiving end, the received reflected power can be represented as

$$\begin{aligned} P_r^{\text{RIS}_{12}}(t) &= \frac{|E_{\text{RIS}_{12}}(t)|^2}{2\eta} S_{r,ap} = P_t G_t G_r\frac{\lambda^2 d_{M_1} d_{N_1} d_{M_2} d_{N_2}}{(4\pi)^4} \\ &\times\left|\sum_{m_2=1}^{M_2}\sum_{n_2=1}^{N_2}\sum_{m_1=1}^{M_1}\sum_{n_1=1}^{N_1}\frac{\chi_{m_1,n_1}(t)\chi_{m_2,n_2}(t)}{\xi_{T,(m_1,n_1)}(t)\xi^{(m_1,n_1)}_{(m_2,n_2)}\xi_{R,(m_2,n_2)}(t)}\right. \\ &\times e^{-j\frac{2\pi}{\lambda}\left(\xi_{T,(m_1,n_1)}(t)+\xi^{(m_1,n_1)}_{(m_2,n_2)}+\xi_{R,(m_1,n_1)}(t)\right)} \\ &\times e^{j\left(\varphi_{m_1,n_1}(t)+\varphi_{m_2,n_2}(t)\right)}\times e^{j\frac{2\pi}{\lambda}v_T t\sin\beta_{T,(m_1,n_1)}(t)\sin\gamma_T} \end{aligned}$$

$$\times e^{j\frac{2\pi}{\lambda}v_T t\cos\left(\alpha_{T,(m_1,n_1)}(t)-\eta_T\right)\cos\beta_{T,(m_1,n_1)}(t)\cos\gamma_T}$$
$$\times e^{j\frac{2\pi}{\lambda}v_R t\cos\left(\alpha_{R,(m_2,n_2)}(t)-\eta_R\right)\cos\beta_{R,(m_2,n_2)}(t)}$$
$$\times\sqrt{\cos\beta^{\text{in}}_{m_1,n_1}(t)\ \cos\beta^{\text{in}}_{(m_1,n_1),(m_2,n_2)}}\Bigg|^2. \tag{51}$$

Consequently, the path power gain of the UAV $\rightarrow$ RIS$_1$ $\rightarrow$ RIS$_2$ $\rightarrow$ GR propagation link, i.e., $\Omega_{\text{TR}}^{\text{RIS}_{12}}(t)$, is expressed as

$$\begin{aligned}&\Omega_{\text{TR}}^{\text{RIS}_{12}}(t)\\&=\mathbb{E}\Bigg\{\frac{\lambda^2 d_{M_1}d_{N_1}d_{M_2}d_{N_2}}{(4\pi)^4}\\&\times\Bigg|\sum_{m_2=1}^{M_2}\sum_{n_2=1}^{N_2}\sum_{m_1=1}^{M_1}\sum_{n_1=1}^{N_1}\frac{\chi_{m_1,n_1}(t)\chi_{m_2,n_2}(t)}{\xi_{T,(m_1,n_1)}(t)\xi^{(m_1,n_1)}_{(m_2,n_2)}\xi_{R,(m_2,n_2)}(t)}\\&\times e^{-j\frac{2\pi}{\lambda}\left(\xi_{T,(m_1,n_1)}(t)+\xi^{(m_1,n_1)}_{(m_2,n_2)}+\xi_{R,(m_1,n_1)}(t)\right)}\\&\times e^{j\left(\varphi_{m_1,n_1}(t)+\varphi_{m_2,n_2}(t)\right)}\times e^{j\frac{2\pi}{\lambda}v_T t\sin\beta_{T,(m_1,n_1)}(t)\sin\gamma_T}\\&\times e^{j\frac{2\pi}{\lambda}v_T t\cos\left(\alpha_{T,(m_1,n_1)}(t)-\eta_T\right)\cos\beta_{T,(m_1,n_1)}(t)\cos\gamma_T}\\&\times e^{j\frac{2\pi}{\lambda}v_R t\cos\left(\alpha_{R,(m_2,n_2)}(t)-\eta_R\right)\cos\beta_{R,(m_2,n_2)}(t)}\\&\times\sqrt{\cos\beta^{\text{in}}_{m_1,n_1}(t)\ \cos\beta^{\text{in}}_{(m_1,n_1),(m_2,n_2)}}\Bigg|^2\Bigg\}.\end{aligned} \tag{52}$$

Similarly, the path power gain of the UAV $\rightarrow$ RIS$_1$ $\rightarrow$ GR propagation link, i.e., $\Omega_{\text{TR}}^{\text{RIS}_1}(t)$, can be expressed as

$$\begin{aligned}&\Omega_{\text{TR}}^{\text{RIS}_1}(t)\\&=\mathbb{E}\Bigg\{\frac{\lambda^2 d_{M_1}d_{N_1}}{(4\pi)^3}\Bigg|\sum_{m_1=1}^{M_1}\sum_{n_1=1}^{N_1}\frac{\chi_{m_1,n_1}(t)e^{j\varphi_{m_1,n_1}(t)}}{\xi_{T,(m_1,n_1)}(t)\xi_{R,(m_1,n_1)}(t)}\\&\times e^{-j\frac{2\pi}{\lambda}\left(\xi_{T,(m_1,n_1)}(t)+\xi_{R,(m_1,n_1)}(t)\right)}\\&\times e^{j\frac{2\pi}{\lambda}v_R t\cos\left(\alpha_{R,(m_1,n_1)}(t)-\eta_R\right)\cos\beta_{R,(m_1,n_1)}(t)}\\&\times e^{j\frac{2\pi}{\lambda}v_T t\cos\left(\alpha_{T,(m_1,n_1)}(t)-\eta_T\right)\cos\beta_{T,(m_1,n_1)}(t)\cos\gamma_T}\\&\times e^{j\frac{2\pi}{\lambda}v_T t\sin\beta_{T,(m_1,n_1)}(t)\sin\gamma_T}\times\sqrt{\cos\beta^{\text{in}}_{m_1,n_1}(t)}\Bigg|^2\Bigg\},\end{aligned} \tag{53}$$

and the path power gain of the UAV $\rightarrow$ RIS$_2$ $\rightarrow$ GR propagation link, i.e., $\Omega_{\text{TR}}^{\text{RIS}_2}(t)$, can be expressed as

$$\begin{aligned}&\Omega_{\text{TR}}^{\text{RIS}_2}(t)\\&=\mathbb{E}\Bigg\{\frac{\lambda^2 d_{M_2}d_{N_2}}{(4\pi)^3}\Bigg|\sum_{m_2=1}^{M_2}\sum_{n_2=1}^{N_2}\frac{\chi_{m_2,n_2}(t)e^{j\varphi_{m_2,n_2}(t)}}{\xi_{T,(m_2,n_2)}(t)\xi_{R,(m_2,n_2)}(t)}\\&\times e^{-j\frac{2\pi}{\lambda}\left(\xi_{T,(m_2,n_2)}(t)+\xi_{R,(m_2,n_2)}(t)\right)}\\&\times e^{j\frac{2\pi}{\lambda}v_R t\cos\left(\alpha_{R,(m_2,n_2)}(t)-\eta_R\right)\cos\beta_{R,(m_2,n_2)}(t)}\\&\times e^{j\frac{2\pi}{\lambda}v_T t\cos\left(\alpha_{T,(m_2,n_2)}(t)-\eta_T\right)\cos\beta_{T,(m_2,n_2)}(t)\cos\gamma_T}\\&\times e^{j\frac{2\pi}{\lambda}v_T t\sin\beta_{T,(m_2,n_2)}(t)\sin\gamma_T}\times\sqrt{\cos\beta^{\text{in}}_{m_2,n_2}(t)}\Bigg|^2\Bigg\}.\end{aligned} \tag{54}$$

In the end, the power gain of the NLoS propagation link through the cluster, i.e., $\Omega_{\text{TR}}^{\text{cluster}}(t)$, can be described as

$$\Omega_{\text{TR}}^{\text{cluster}}(t)=\frac{\lambda^2 P_{\text{cluster},\ell}(t)}{(4\pi)^2\left(\xi_{T,\text{cluster},\ell}(t)+\xi_{R,\text{cluster},\ell}(t)\right)^2}, \tag{55}$$

where $P_{\text{cluster},\ell}(t)=\exp\big(-\tau^{\text{cluster}}(t)\frac{r_\tau-1}{r_\tau\sigma_\tau}\big)\cdot 10^{\frac{-Z_{\text{cluster},\ell}}{10}}$ represents the cluster power. Here, r_τ and σ_τ represent the delay scale parameter and delay spread, respectively; $Z_{\text{cluster},\ell}$ is a stochastic variable satisfying Gaussian distribution, i.e., $Z_{\text{cluster},\ell}\sim\mathcal{N}(0,\zeta^2)$, and its values can be gathered from Table 7.5.6 in [27].

REFERENCES

[1] C. X. Wang, J. Huang, H. Wang, X. Gao, X. You, and Y. Hao, "6G wireless channel measurements and models: Trends and challenges," *IEEE Veh. Technol. Mag.*, vol. 15, no. 4, pp. 22–32, Dec. 2020.

[2] E. Basar and I. Yildirim, "Reconfigurable intelligent surfaces for future wireless networks: A channel modeling perspective," *IEEE Wireless Commun.*, vol. 28, no. 3, pp. 108–114, Jun. 2021.

[3] R. Faqiri, C. Saigre-Tardif, G. C. Alexandropoulos, N. Shlezinger, M. F. Imani, and P. del Hougne, "PhysFad: Physics-based end-to-end channel modeling of RIS-parametrized environments with adjustable fading," *IEEE Trans. Wireless Commun.*, vol. 22, no. 1, pp. 580–595, Jan. 2023.

[4] H. Jiang, M. Mukherjee, J. Zhou, and J. Lloret, "Channel modeling and characteristics analysis for 6G wireless communications," *IEEE Netw.*, vol. 35, no. 1, pp. 296–303, Jan. 2021.

[5] L. Zeng, X. Cheng, C.-X. Wang, and X. Yin, "A 3D geometry-based stochastic channel model for UAV-MIMO channels," in *Proc. IEEE Wireless Commun. Netw. Conf. (WCNC)*, San Francisco, CA, USA, Mar. 2017, pp. 1–5.

[6] Y. Li and X. Cheng, "New deterministic and statistical simulation models for non-isotropic UAV-MIMO channels," in *Proc. WCSP*, Nanjing, China, 2017, pp. 1–6.

[7] H. Jiang, Z. Zhang, and G. Gui, "Three-dimensional non-stationary wideband geometry-based UAV channel model for A2G communication environments," *IEEE Access*, vol. 7, pp. 26116–26122, 2019.

[8] Z. Ma et al., "Impact of UAV rotation on MIMO channel characterization for air-to-ground communication systems," *IEEE Trans. Veh. Technol.*, vol. 69, no. 11, pp. 12418–12431, Nov. 2020.

[9] S. Li, B. Duo, X. Yuan, Y.-C. Liang, and M. Di Renzo, "Reconfigurable intelligent surface assisted UAV communication: Joint trajectory design and passive beamforming," *IEEE Wireless Commun. Lett.*, vol. 9, no. 5, pp. 716–720, Jan. 2020.

[10] H. Jiang, R. S. He, C. Ruan, J. Zhou, and D. Chang, "Three-dimensional geometry-based stochastic channel modeling for intelligent reflecting surface-assisted UAV MIMO communications," *IEEE Wireless Commun. Lett.*, vol. 10, no. 12, pp. 2727–2731, Dec. 2021.

[11] B. Xiong, Z. Zhang, H. Jiang, J. Zhang, L. Wu, and J. Dang, "A 3D non-stationary MIMO channel model for reconfigurable intelligent surface auxiliary UAV-to-ground mmWave communications," *IEEE Trans. Wireless Commun.*, vol. 21, no. 7, pp. 5658–5672, Jul. 2022.

[12] C. Cao, Z. Lian, Y. Wang, Y. Su, and B. Jin, "A non-stationary geometry-based channel model for IRS-assisted UAV-MIMO channels," *IEEE Commun. Lett.*, vol. 25, no. 12, pp. 3760–3764, Dec. 2021.

[13] Z. Abdullah, A. Papazafeiropoulos, S. Kisseleff, S. Chatzinotas, and B. Ottersten, "Impact of phase-noise and spatial correlation on double-RIS-assisted multiuser MISO networks," *IEEE Wireless Commun. Lett.*, vol. 11, no. 7, pp. 1473–1477, Jul. 2022.

[14] Y. Han, S. Zhang, L. Duan, and R. Zhang, "Double-IRS aided MIMO communication under LoS channels: Capacity maximization and scaling," *IEEE Trans. Commun.*, vol. 70, no. 4, pp. 2820–2837, Apr. 2022.

[15] Y. Han, S. Zhang, L. Duan, and R. Zhang, "Cooperative double-IRS aided communication: Beamforming design and power scaling," *IEEE Wireless Commun. Lett.*, vol. 9, no. 8, pp. 1206–1210, Aug. 2020.

[16] B. Zheng, C. You, and R. Zhang, "Double-IRS assisted multi-user MIMO: Cooperative passive beamforming design," *IEEE Trans. Wireless Commun.*, vol. 20, no. 7, pp. 4513–4526, Jul. 2021.

[17] J. Li, M. Fu, Y. Zhou, and Y. Shi, "Double-RIS assisted over-the-air computation," in *Proc. IEEE Globecom Workshops*, Madrid, Spain, vol. 2021, pp. 1–6.

[18] B. Xiong, Z. Zhang, and H. Jiang, "Reconfigurable intelligent surface for mmWave mobile communications: What if LoS path exists?" *IEEE Wireless Commun. Lett.*, vol. 12, no. 2, pp. 247–251, Feb. 2023.

[19] Z. Abdullah, S. Kisseleff, K. Ntontin, W. A. Martins, S. Chatzinotas, and B. Ottersten, "Double-RIS communication with DF relaying for coverage extension: Is one relay enough?" in *Proc. IEEE Int. Conf. Commun.*, Seoul, South Korea, May 2022, pp. 2639–2644.

[20] H. Jiang et al., "A novel 3D UAV channel model for A2G communication environments using AoD and AoA estimation algorithms," *IEEE Trans. Commun.*, vol. 68, no. 11, pp. 7232–7246, Nov. 2020.
[21] B. Xiong et al., "A statistical MIMO channel model for reconfigurable intelligent surface assisted wireless communications," *IEEE Trans. Commun.*, vol. 70, no. 2, pp. 1360–1375, Feb. 2022.
[22] A. Goldsmith, *Wireless Communications*, Cambridge, U.K.: Cambridge Univ. Press, 2005.
[23] *Study on Enhanced LTE Support for Aerial Vehicles*, 3GPP, document TR 36.777, Dec. 2017.
[24] H. Jiang, Z. Zhang, L. Wu, and J. Dang, "Three-dimensional geometry-based UAV-MIMO channel modeling for A2G communication environments," *IEEE Commun. Lett.*, vol. 22, no. 7, pp. 1438–1441, Jul. 2018.
[25] C. F. López and C.-X. Wang, "Novel 3-D non-stationary wideband models for massive MIMO channels," *IEEE Trans. Wireless Commun.*, vol. 17, no. 5, pp. 2893–2905, May 2018.
[26] Y. Sun, C.-X. Wang, J. Huang, and J. Wang, "A 3D non-stationary channel model for 6G wireless systems employing intelligent reflecting surfaces with practical phase shifts," *IEEE Trans. Cogn. Commun. Netw.*, vol. 7, no. 2, pp. 496–510, Jun. 2021.
[27] *Study on Channel Model for Frequencies Form 0.5 to 100 GHz*, 3GPP, document TR 38.901, 2019.
[28] H. Jiang et al., "A general wideband non-stationary stochastic channel model for intelligent reflecting surface-assisted MIMO communications," *IEEE Trans. Wireless Commun.*, vol. 20, no. 8, pp. 5314–5328, Aug. 2021.
[29] S. Payami and F. Tufvesson, "Channel measurements and analysis for very large array systems at 2.6 GHz," in *Proc. EUCAP*, Prague, Czech Republic, Mar. 2012, pp. 433–437.
[30] J. Bian, C.-X. Wang, X. Q. Gao, X. You, and M. Zhang, "A general 3D non-stationary wireless channel model for 5G and beyond," *IEEE Trans. Wireless Commun.*, vol. 20, no. 5, pp. 3211–3224, May 2021.
[31] G. Sun et al., "A 3D wideband channel model for RIS-assisted MIMO communications," *IEEE Trans. Veh. Technol.*, vol. 71, no. 8, pp. 8016–8029, Aug. 2022.
[32] C. A. Balanis, *Antenna Theory: Analysis and Design*. Hoboken, NJ, USA: Wiley, 2016.
[33] W. L. Stutzman and G. A. Thiele, *Antenna Theory and Design*. Hoboken, NJ, USA: Wiley, 2013.

Hao Jiang (Member, IEEE) received the B.S. and M.S. degrees in electrical and information engineering from the Nanjing University of Information Science and Technology, Nanjing, China, in 2012 and 2015, respectively, and the Ph.D. degree from Southeast University, Nanjing, in 2019. From 2017 to 2018, he was a Visiting Student with the Department of Electrical Engineering, Columbia University in the City of New York, New York, NY, USA. He is currently an Associate Professor with the School of Artificial Intelligence/School of Future Technology, Nanjing University of Information Science and Technology. His current research interests include wireless channel measurements and modeling, 6G wireless communication networks, signal processing, machine learning, and AI-driven technologies.

Baiping Xiong received the B.Eng. degree in information engineering from Southeast University, Nanjing, China, in 2019, where he is currently pursuing the Ph.D. degree with the National Mobile Communications Research Laboratory.

Hongming Zhang (Member, IEEE) received the B.Eng. degree (Hons.) in telecommunications from the Nanjing University of Aeronautics and Astronautics (NUAA) and the City University of London in 2011, and the M.Sc. and Ph.D. degrees in wireless communications from the University of Southampton in 2012 and 2017, respectively. From 2017 to 2018, he was with the Department of Electrical Engineering, Columbia University, New York, NY, USA. He is currently an Assistant Professor with the School of Information and Communication Engineering, Beijing University of Posts and Telecommunications, Beijing, China. His research interests include wireless communications, heterogeneous network performance analysis and optimization, and machine learning.

Ertugrul Basar (Fellow, IEEE) received the Ph.D. degree from Istanbul Technical University in 2013. He had visiting positions with Ruhr University Bochum, Germany, as a Mercator Fellow, in 2022, and Princeton University, USA, as a Visiting Research Collaborator, from 2011 to 2012. He is currently an Associate Professor with the Department of Electrical and Electronics Engineering, Koç University, Istanbul, Turkey, and the Director of the Communications Research and Innovation Laboratory (CoreLab). His research interests include beyond 5G and 6G wireless networks, communication theory and systems, reconfigurable intelligent surfaces, index modulation, waveform design, and signal processing for communications. He was a Young Member of the Turkish Academy of Sciences in 2017. In the past, he served as an Editor/Senior Editor for many journals, including IEEE COMMUNICATIONS LETTERS (2016–2022), IEEE TRANSACTIONS ON COMMUNICATIONS (2018–2022), *Physical Communication* (2017–2020), and IEEE ACCESS (2016–2018). He is also an Editor of *Frontiers in Communications and Networks*.